Inorganic Chemistry

Article

pubs.acs.org/IC

Synthesis, Structure, and Characterization of Dinuclear Copper(I) Halide Complexes with P^N Ligands Featuring Exciting Photoluminescence Properties

Daniel M. Zink,[†,‡] Michael Bächle,[‡] Thomas Baumann,*[,‡] Martin Nieger,[§] Michael Kühn,[∥] Cong Wang,[∥] Wim Klopper,[∥] Uwe Monkowius,*[,⊥] Thomas Hofbeck,[#] Hartmut Yersin,*[,#] and Stefan Bräse*[,†]

[†]Institute of Organic Chemistry, Karlsruhe Institute of Technology, KIT Campus South, Fritz-Haber-Weg 6, D-76131 Karlsruhe, Germany

[‡]cynora GmbH, Hermann-von-Helmholtz-Platz 1, D-76344 Eggenstein-Leopoldshafen, Germany

[§]Laboratory of Inorganic Chemistry, University of Helsinki, P.O. Box 55, FIN-00014, Germany

[∥]Institute of Physical Chemistry, Karlsruhe Institute of Technology, KIT Campus South, Fritz-Haber-Weg 2, D-76131 Karlsruhe, Germany

[⊥]Institute of Inorganic Chemistry, Johannes Kepler University Linz, Altenbergerstrasse 69, A-4040 Linz, Austria

[#]Institute of Physical Chemistry, University of Regensburg, Universitätsstrasse 31, D-93053 Regensburg, Germany

Supporting Information

ABSTRACT: A series of highly luminescent dinuclear copper(I) complexes has been synthesized in good yields using a modular ligand system of easily accessible diphenylphosphinopyridine-type P^N ligands. Characterization of these complexes via X-ray crystallographic studies and elemental analysis revealed a dinuclear complex structure with a butterfly-shaped metal-halide core. The complexes feature emission covering the visible spectrum from blue to red together with high quantum yields up to 96%. Density functional theory calculations show that the HOMO consists mainly of orbitals of both the metal core and the bridging halides, while the LUMO resides dominantly on the heterocyclic part of the P^N ligands. Therefore, modification of the heterocyclic moiety of the bridging ligand allows for systematic tuning of the luminescence wavelength. By increasing the aromatic system of the N-heterocycle or through functionalization of the pyridyl moiety, complexes with emission maxima from 481 to 713 nm are obtained. For a representative compound, it is shown that the ambient-temperature emission can be assigned as a thermally activated delayed fluorescence, featuring an attractively short emission decay time of only 6.5 μs at ϕ_{PL} = 0.8. It is proposed to apply these compounds for singlet harvesting in OLEDs.

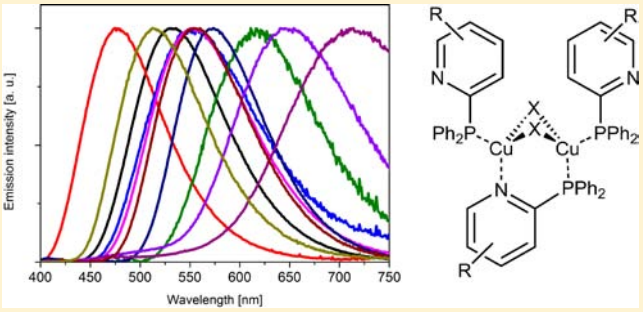

1. INTRODUCTION

In the past decade, substantial research has been focused on new energy-saving concepts for lighting and display applications. Organic light-emitting diodes (OLEDs) are the most promising devices for these task, since they consume only a fraction of the energy of conventional, inefficient light bulbs and can be manufactured on thin, flexible, and lightweight substrates.[1,2] Significant progress has been achieved in both increasing the efficiency and allowing for color tuning by use of emitters based on Ir,[3−11] Pt,[10,12−18] and Os[19−22] because with these both triplet and singlet excitons formed upon charge recombination in the emissive layer can be utilized.[2,23] These materials, however, are produced from rather expensive metals, which is one reason why more abundant and cost-efficient metals with d^{10} configuration such as Cu(I), Ag(I), or Au(I) have received more attention recently.[24−28] Out of this group luminescent copper(I) complexes have attracted increasing interest due to their rich structural and photophysical properties.[29−47] After the pioneering work of McMillin, Ford, and Eisenberg on mostly cationic mononuclear Cu(I) complexes, it is well known that these compounds frequently feature metal-to-ligand charge-transfer (MLCT) absorption bands in the visible part of the spectrum which can be regarded as a formal oxidation of Cu(I) to Cu(II) in the excited state.[33−47] According to this type of electronic transition, usually a geometry change occurs from a pseudotetrahedral coordination with a flattening tendency toward a square-planar coordination. In addition to this geometrical distortion being a major quenching pathway of the emission, the complexes are vulnerable to solvent coordination and exciplex formation, resulting in additional quenching pathways. This frequently

Received: May 11, 2012
Published: October 12, 2012

leads to low quantum yields for these compounds in solution.[48−51]

One way to address the aforementioned problems is the use of trigonal-planar complexes with rigid ligands which hamper the Jahn-Teller distortion from a Y- to a T-shaped geometry upon excitation, yielding complexes with high emission quantum yields.[43] However, with respect to the emission of the triplet states and the long phosphorescence decay times, which are related to the relatively weak spin-orbit coupling of the copper atom,[42,52] application in OLEDs is problematic. On the other hand, low singlet−triplet splitting found for several Cu(I) compounds allows for emission from both the singlet and the triplet excited state depending on the temperature.[44,46,47] The singlet excited state, which is slightly higher in energy than the triplet state, can be thermally activated at the expense of the triplet state, leading to the so-called thermally activated delayed fluorescence (TADF).[44,46,47,53−57] With respect to electroluminescent applications, this concept is termed "singlet harvesting", in contrast to the "triplet harvesting", being of importance if Ir(III)- and Pt(II)-based emitters are used.[47] Even though the excited-state lifetime is much shorter for emission from the singlet state than from the triplet state, the equilibrium between those two states has to be taken into account. Nevertheless, the overall emission decay time is still much shorter than that of the triplet state.[44,46,47] Moreover, it has been shown that increased structural rigidity reduces radiationless deactivation pathways in mononuclear copper(I) complexes leading to strongly enhanced quantum yields,[44,46,47] which may also be expected for rigid clusters.[58] First examples confirm the suitability of such Cu(I) complexes as emitters in OLEDs,[31,43,51,59,60] whereas the processability is frequently still a challenge and under investigation.[61]

In this study, we present a series of highly luminescent dinuclear copper(I) complexes bearing bridging P^N ligands. The ligands consist of N-heterocycles with a diphenylphosphino group and allow for easy tuning of both the emission color as well as the solubility of the complexes. Furthermore, the electronic structures of these compounds are investigated using ab initio calculations. In particular, the HOMO can be mostly assigned to the copper(I)-halide core, while the LUMO mainly resides on the chelating ligand and can therefore be tuned to achieve different emission colors. For a representative compound, it will be shown that the ambient-temperature emission can be assigned as thermally activated delayed fluorescence. This implies the high potential of these materials for OLED applications.

2. EXPERIMENTAL SECTION

General Procedures. All reactions were performed in oven-dried glassware under an argon atmosphere. Solvents and chemicals used were purchased from commercial suppliers. Solvents were dried under standard conditions. All materials were used without further purification. Thin-layer chromatography (TLC) was carried out on silica gel plates (Silica gel 60, F254, Merck) with detection by UV. Purification was performed with preparative chromatography using normal-phase silica gel (Silica gel 60, 230−400 mesh, Merck). ^{1}H NMR, ^{13}C NMR, and ^{31}P NMR were recorded on Bruker AM 400 and Bruker DRX 250. Chemical shifts are reported as δ values (ppm). Signal abbreviations include s = singlet, bs = broad singlet, d = doublet, t = triplet, q = quartet, quin = quintet, m = multiplet, Ar-H = aromatic proton. Signals of ^{13}C NMR spectra were allocated through DEPT technology (DEPT = distortionless enhancement by polarization transfer). The signal abbreviations include C-Ar = aromatic carbon, + = primary or tertiary carbon, − = secondary carbon, C_{quart} = quaternary carbon. MS (EI) (electron impact mass spectrometry), FAB (fast atom bombardment mass spectrometry), and HRMS (high-resolution mass spectrometry) were carried out on a Finnigan MAT 90 (70 eV). Molecular fragments are quoted as the relation between mass and charge (m/z) and the intensities as a percentage value relative to the intensity of the base signal (100%). The abbreviation [M$^+$] refers to the molecular ion. Descriptions without nominated temperature were done at room temperature (rt), and the following abbreviations were used: calcd (theoretical value), found (measured value). Information is given in mass percent. IR (infrared spectroscopy) was carried out on a FT-IR Bruker IFS 88. IR spectra of solids were recorded in KBr and as thin films on KBr for oils and liquids. The deposit of the absorption band was given in wavenumbers $\tilde{\nu}$ in cm^{-1}. Forms and intensities of the bands were characterized as follows: s = strong 10−40% transmission, m = medium 40−70% transmission, w = weak 70−90% transmission, vw = very weak 90−100% transmission, br = broad

Synthesis of P^N-Type Ligands. Spectroscopic data of ligands **1**,[63] **2**,[62] **6**,[64] **8**,[65] and **11**[66] have already been published in the literature; for spectroscopic data of ligands **3**−**5**, **7**, **9**, and **12**−**17** see Supporting Information.

*I. General Procedure for Substitution of Halide Substituents (Cl, Br) by Reaction with Lithium Diphenylphosphanide Yielding Compounds **3**−**11**.* Lithium (21.6 mmol, 2.16 equiv) was suspended under a nitrogen atmosphere in dry tetrahydrofuran (50 mL) at 0 °C. Chlorodiphenylphosphane (11.0 mmol, 1.10 equiv) dissolved in tetrahydrofuran (15 mL) was added dropwise via cannula, and the mixture was stirred at room temperature overnight. To the resulting deep red solution was added the respective aryl chloride, fluoride, or bromide (10.0 mmol, 1.00 equiv) dropwise via cannula at room temperature. The mixture was stirred for 8 h at room temperature and, after quenching with water (2 mL), filtered through a plug of silica gel. Purification via flash column chromatography yielded the product.

*II. General Procedure for Alkylation of 4-Methyl-2-(diphenylphosphino)pyridine (**10**) Yielding Compounds **13**−**17**.* Under a nitrogen atmosphere 4-methyl-2-(diphenylphosphino)-pyridine (**10**) (4.00 mmol, 1.00 equiv) was dissolved in dry tetrahydrofuran and cooled to −78 °C. Lithium diisopropylamine (1.8 M in tetrahydrofuran, 6.00 mmol, 1.50 equiv) was added dropwise via cannula. The reaction mixture was stirred at −78 °C for 60 min, afterward at room temperature for 1 h, and then cooled again to −78 °C. The electrophile (6.00 mmol, 1.50 equiv) was added dropwise via cannula, and the resulting mixture was allowed to warm to room temperature. After quenching with water (2 mL), the mixture was filtered through a plug of silica gel. Purification via flash column chromatography yielded the product.

*III. General Procedure for Ortho-Lithiation of Pyridine Derivatives to Synthesize Compounds **2** and **12**.* A solution of *N,N*-dimethylethanolamine (27.4 mmol, 2.00 equiv) in *n*-hexane (25 mL) was cooled to −5 °C, and *n*-butyllithium (54.9 mmol, 4.00 equiv) was added dropwise. After stirring at this temperature for 15 min, a solution of the pyridine derivate (13.7 mmol, 1.00 equiv) in *n*-hexane (10 mL) was added dropwise via canula. The resulting solution was stirred at −5 °C for another 5 min, and hereafter, the reaction mixture was cooled to −80 °C and a solution of chlorodiphenylphosphane (34.3 mmol, 2.50 equiv) was added dropwise. The reaction mixture was allowed to warm to room temperature, and after quenching with water (2 mL), the reaction mixture was filtered through a plug of silica gel. Purification via flash column chromatography yielded the product.

General Procedure for the Syntheses of Complexes 1-I−17-I. The copper(I) halide salt (2.00 equiv) and the ligand (3.00 equiv) were suspended under nitrogen in dry dichloromethane (10 mL) and stirred for 12 h at room temperature resulting in a clear solution. Afterward the complex was purified through precipitation with diethyl ether, pentane, or cyclohexane (100 mL). The solid was filtered off, washed with the appropriate solvent, and dried in vacuum.

*[(2-(Diphenylphosphino)pyridine)$_3$Cu$_2$I$_2$] (**1-I**).* Yield: 591 mg, 0.51 mmol, 80%; yellow powder. IR (ATR): $\tilde{\nu}$ = 1570 (w), 1480 (w), 1452 (w), 1433 (w), 1419 (w), 1092 (w), 743 (m), 694 (m), 506 (m), 492 (m), 421 (w) cm^{-1}. MS (FAB): Due to insolubility of the compound,

dx.doi.org/10.1021/ic300979c | Inorg. Chem. 2013, 52, 2292−2305

no mass spectra could be measured. Anal. Calcd for $C_{51}H_{42}Cu_2I_2N_3P_3$ (1168.9): C, 52.32; H, 3.62; N, 3.59. Found: C, 52.07; H, 3.57; N, 3.49.

*[(2-(Diphenylphosphino)pyridine)$_3$Cu$_2$Br$_2$] (**1-Br**).* Yield: 507 mg, 0.47 mmol, 75%; yellow powder. IR (ATR): $\tilde{\nu}$ = 1570 (w), 1480 (w), 1453 (w), 1434 (w), 1420 (w), 1094 (w), 767 (w), 742 (m), 693 (m), 504 (m), 491 (m), 437 (w), 421 (w) cm^{-1}. MS (FAB), *m*/*z* (%): 996 (1), 733 (2), 589 (5), 470 (8), 326 (13), 154 (100). Anal. Calcd for $C_{51}H_{42}Cu_2Br_2N_3P_3$ (1072.9): C, 57.04; H, 3.92; N, 3.78. Found: C, 56.89; H, 3.93; N, 3.90.

*[(2-(Diphenylphosphino)pyridine)$_3$Cu$_2$Cl$_2$] (**1-Cl**).* Yield: 453 mg, 0.46 mmol, 73%; yellow powder. IR (ATR): $\tilde{\nu}$ = 1569 (w), 1479 (w), 1452 (w), 1434 (w), 1420 (w), 1093 (w), 987 (w), 767 (w), 742 (m), 692 (m), 502 (m), 490 (m), 436 (w), 421 (w) cm^{-1}. MS (FAB), *m*/*z* (%): 787 (2), 687 (32), 589 (51), 426 (45) 326 (100). Anal. Calcd for $C_{51}H_{42}Cu_2Cl_2N_3P_3 \cdot 1/4CH_2Cl_2$ (1059.1): C, 61.00; H, 4.25; N, 4.16. Found: C, 61.03; H, 4.29; N, 3.93.

*[(2-(Diphenylphosphino)-N,N-dimethylpyridine-4-amine)$_3$Cu$_2$I$_2$] (**2-I**).* Yield: 421 mg, 0.32 mmol, 60%; white powder. IR (ATR): $\tilde{\nu}$ = 1588 (w), 1433 (vw), 1376 (vw), 1224 (vw), 1094 (vw), 999 (vw), 984 (vw), 812 (vw), 739 (vw), 691 (w), 525 (w), 501 (w), 467 (w), 425 (vw) cm^{-1}. MS (FAB), *m*/*z* (%): 1170 (1), 1056 (6), 865 (35), 675 (34), 559 (42), 369 (100), 307 (31). Anal. Calcd for $C_{57}H_{57}Cu_2I_2N_6P_3$ (1298.0): C, 52.67; H, 4.42; N, 6.47. Found: C, 52.39; H, 4.44; N, 6.38.

*[(2-(Diphenylphosphino)-6-fluoropyridine)$_3$Cu$_2$I$_2$] (**3-I**).* Yield: 548 mg, 0.45 mmol, 76%; yellow powder. IR (ATR): $\tilde{\nu}$ = 1584 (w), 1567 (w), 1480 (w), 1433 (m), 1253 (w), 1093 (w), 988 (w), 896 (w), 800 (w), 742 (w), 691 (m), 617 (w), 518 (m), 496 (m) cm^{-1}. MS (FAB), *m*/*z* (%): 1006 (1), 816 (3), 723 (1), 625 (10), 534 (3), 344 (10). Anal. Calcd for $C_{51}H_{39}Cu_2F_3I_2N_3P_3$ (1222.9): C, 50.02; H, 3.21; N, 3.43. Found: C, 50.17; H, 3.29; N, 3.42.

*[(2-(Diphenylphosphino)-4,6-dimethylquinoline)$_3$Cu$_2$I$_2$] (**4-I**).* Yield: 509 mg, 0.36 mmol, 74%; ochre powder. IR (ATR): $\tilde{\nu}$ = 1582 (w), 1545 (vw), 1481 (vw), 1434 (w), 1377 (w), 1094 (w), 882 (vw), 823 (w), 742 (w), 692 (m), 534 (w), 508 (w), 451 (w), 420 (w) cm^{-1}. MS (FAB), *m*/*z* (%): 1316 (<1), 1127 (2), 937 (19), 845 (7), 745 (30), 594 (22), 404 (68), 342 (100). Anal. Calcd for $C_{69}H_{60}Cu_2I_2N_3P_3$ (1403.1): C, 58.98; H, 4.30; N, 2.99. Found: C, 59.52; H, 4.78; N, 2.73.

*[(3-(Diphenylphosphino)isoquinoline)$_3$Cu$_2$I$_2$] (**5-I**).* Yield: 303 mg, 0.23 mmol, 72%; yellow powder. IR (ATR): $\tilde{\nu}$ = 1569 (vw), 1481 (vw), 1433 (w), 1276 (vw), 1095 (w), 885 (vw), 746 (w), 692 (m), 661 (w), 514 (w), 475 (w), 449 (w) cm^{-1}. MS (FAB), *m*/*z* (%): 1193 (1), 1070 (3), 878 (4), 757 (1), 689 (3), 566 (5), 376 (10). Anal. Calcd for $C_{63}H_{48}Cu_2I_2N_3P_3 \cdot 1/2CH_2Cl_2$ (1320.9): C, 55.94; H, 3.62; N, 3.08. Found: C, 55.51; H, 3.66; N, 2.98.

*[(1-(Diphenylphosphino)isoquinoline)$_3$Cu$_2$I$_2$] (**6-I**).* Yield: 156 mg, 0.12 mmol, 28%; red powder. IR (ATR): $\tilde{\nu}$ = 1545 (w), 1480 (w), 1434 (w), 1306 (w), 1097 (w), 827 (w), 741 (m), 692 (m), 540 (m), 521 (w), 487 (m), 461 (m) cm^{-1}. MS (FAB), *m*/*z* (%): 1068 (8), 879 (4), 757 (16), 689 (32), 566 (19), 376 (100). Anal. Calcd for $C_{63}H_{48}Cu_2I_2N_3P_3 \cdot 1.5CH_2Cl_2$ (1444.9): C, 53.49; H, 3.55; N, 2.90. Found: C, 53.99; H, 2.95; N, 3.23.

*[(2-(Diphenylphosphino)quinoxaline)$_3$Cu$_2$I$_2$] (**7-I**).* Yield: 582 mg, 0.44 mmol, 83%; orange powder. IR (ATR): $\tilde{\nu}$ = 1483 (w), 1434 (w), 1365 (vw), 1090 (w), 964 (w), 758 (m), 742 (m), 691 (m), 626 (w), 509 (m), 485 (m), 402 (m) cm^{-1}. MS (FAB), *m*/*z* (%): 1263 (1), 1073 (3), 881 (8), 691 (18), 567 (15), 377 (31), 155 (100). Anal. Calcd for $C_{60}H_{45}Cu_2I_2N_6P_3 \cdot CH_2Cl_2$ (1409.9): C, 52.01; H, 3.36; N, 5.97. Found: C, 51.78; H, 3.42; N, 5.84.

*[(2-(Diphenylphosphino)benzo[d]thiazole)$_3$Cu$_2$I$_2$] (**8-I**).* Yield: 598 mg, 0.45 mmol, 86%; yellow powder. IR (ATR): $\tilde{\nu}$ = 1450 (w), 1432 (w), 1311 (w), 1092 (w), 985 (w), 849 (vw), 758 (m), 739 (m), 690 (m), 601 (w), 580 (w), 506 (m), 487 (m) cm^{-1}. MS (FAB), *m*/*z* (%): 1211 (4), 1082 (4), 892 (15), 763 (4), 701 (5), 572 (21), 382 (18). Anal. Calcd for $C_{57}H_{42}Cu_2I_2N_3P_3S_3$ (1336.8): C, 51.13; H, 3.16; N, 3.14; S, 7.18. Found: C, 51.19; H, 3.34; N, 3.05; S, 6.57.

*[(2-(Diphenylphosphino)-6-methylbenzo[d]thiazole)$_3$Cu$_2$I$_2$] (**9-I**).* Yield: 530 mg, 0.38 mmol, 61%; yellow powder. IR (ATR): $\tilde{\nu}$ = 3047 (vw), 1596 (vw), 1482 (vw), 1464 (vw), 1433 (w), 1310 (vw), 1236 (vw), 1157 (vw), 1093 (vw), 1028 (vw), 1028 (vw) 999 (vw), 811 (w), 739 (w), 690 (w), 604 (vw), 505 (m), 457 (w), 428 (w) cm^{-1}. MS (FAB), *m*/*z* (%): 1380 (1), 1253 (9), 921 (43), 729 (11), 586 (42), 460 (7), 396 (28), 154 (100). Anal. Calcd for $C_{60}H_{48}Cu_2I_2N_3P_3S_3 \cdot 1/4CH_2Cl_2$ (1378.9): C, 51.60; H, 3.49; N, 3.00; S, 6.86. Found: C, 51.38; H, 3.55; N, 2.75; S, 6.85.

*[(2-(Diphenylphosphino)-4-methylpyridine)$_3$Cu$_2$I$_2$] (**10-I**).* Yield: 516 mg, 0.43 mmol, 71%; yellow powder. IR (ATR): $\tilde{\nu}$ = 1775 (vw), 1585 (vw), 1432 (w), 1225 (w), 1191 (w), 1161 (w), 1090 (w), 826 (w), 741 (w), 691 (w), 510 (w), 495 (w), 460 (w), 426 (w) cm^{-1}. MS (FAB), *m*/*z* (%): 996 (32), 809 (23), 721 (31), 617 (33), 530 (55), 340 (100). Anal. Calcd for $C_{54}H_{48}Cu_2I_2N_3P_3$ (1210.9): C, 53.48; H, 3.99; N, 3.46. Found: C, 53.09; H, 3.95; N, 3.39.

*[(2-(Diphenylphosphino)-6-methylpyridine)$_3$CuI] (**11-I**).* Yield: 325 mg, 0.32 mmol, 53%; white powder. IR (ATR): $\tilde{\nu}$ = 1583 (w), 1557 (vw), 1434 (w), 1094 (w), 810 (vw), 738 (w), 726 (w), 690 (m), 567 (w), 517 (w), 494 (w), 453 (w) cm^{-1}. MS (FAB), *m*/*z* (%): 998 (6), 896 (3) [L_3Cu^+], 809 (36), 617 (100) [L_2Cu^+], 530 (38), 340 (96) [LCu^+], 294 (50). Anal. Calcd for $C_{54}H_{48}CuIN_3P_3 \cdot 2/3CH_2Cl_2$ (1210.9): C, 60.85; H, 4.61; N, 3.89. Found: C, 60.88; H, 4.72; N, 3.89.

*[(2-(Diphenylphosphino)-3,5-dimethylpyridine)Cu$_2$I$_2$] (**12-I**).* Yield: 149 mg, 0.12 mmol, 35%; yellow powder. IR (ATR): $\tilde{\nu}$ = 1480 (w), 1434 (w), 1389 (w), 1094 (w), 1027 (w), 740 (m), 692 (m), 625 (w), 544 (w), 509 (m), 491 (m), 468 (w) cm^{-1}. MS (FAB), *m*/*z* (%): 1082 (8), 1005 (9), 893 (9), 814 (15), 764 (29), 737 (18), 624 (82), 547 (100), 495 (29), 382 (82), 242 (44). Anal. Calcd for $C_{57}H_{54}Cu_2I_2N_3P_3 \cdot 1/2CH_2Cl_2$ (1253.0): C, 53.23; H, 4.27; N, 3.24. Found: C, 53.15; H, 4.40; N, 2.88.

*[(2-(Diphenylphosphino)-4-propylpyridine)$_3$Cu$_2$I$_2$] (**13-I**).* Yield: 455 mg, 0.35 mmol, 80%; yellow powder. IR (ATR): $\tilde{\nu}$ = 1588 (w), 1481 (w), 1434 (w), 1390 (w), 1094 (w), 989 (vw), 825 (vw), 741 (w), 693 (m), 513 (m), 497 (m), 470 (w) cm^{-1}. MS (FAB), *m*/*z* (%): 1244 (4), 1055 (8), 865 (26), 750 (7), 673 (22), 558 (55), 368 (100). Anal. Calcd for $C_{60}H_{60}Cu_2I_2N_3P_3 \cdot 1/4CH_2Cl_2$ (1295.1): C, 54.90; H, 4.63; N, 3.19. Found: C, 54.90; H, 4.95; N, 3.01.

*[(2-(Diphenylphosphino)-4-isobutylpyridine)$_3$Cu$_2$I$_2$] (**14-I**).* Yield: 452 mg, 0.34 mmol, 65%; yellow powder. IR (ATR): $\tilde{\nu}$ = 2953 (w), 1586 (w), 1542 (w), 1480 (w), 1461 (w), 1433 (w), 1384 (w), 1091 (w), 739 (w), 690 (m), 508 (m), 494 (m), 481 (m) cm^{-1}. MS (FAB), *m*/*z* (%): 1082 (44), 893 (17), 763 (38), 701 (25), 572 (54), 382 (100). Anal. Calcd for $C_{63}H_{66}Cu_2I_2N_3P_3$ (1337.1): C, 56.51; H, 4.97; N, 3.14. Found: C, 56.72; H, 4.96; N, 3.10.

*[(2-(Diphenylphosphino)-4-heptylpyridine)$_3$Cu$_2$I$_2$] (**15-I**).* Yield: 343 mg, 0.23 mmol, 51%; yellow powder. IR (ATR): $\tilde{\nu}$ = 2919 (vw), 2850 (vw), 1586 (vw), 1432 (w), 1389 (vw), 1095 (vw), 989 (vw), 739 (w), 692 (w), 513 (w), 497 (w), 460 (w) cm^{-1}. MS (FAB), *m*/*z* (%): 1355 (2), 1166 (11), 976 (17), 805 (17), 785 (44), 613 (59), 424 (100), 362 (16). Anal. Calcd for $C_{72}H_{84}Cu_2I_2N_3P_3$ (1463.2): C, 59.02; H, 5.78; N, 2.87. Found: C, 58.91; H, 5.64; N, 2.85.

*[(2-(Diphenylphosphino)-4-cyclopentylmethylpyridine)$_3$Cu$_2$I$_2$] (**16-I**).* Yield: 387 mg, 0.27 mmol, 57%; yellow powder. IR (ATR): $\tilde{\nu}$ = 2948 (w), 1588 (w), 1434 (w), 1094 (w), 753 (w), 740 (w), 695 (w), 518 (w), 496 (m), 518 (m), 496 (m), 429 (w) cm^{-1}. MS (FAB), *m*/*z* (%): 1134 (15), 943 (14), 787 (33), 753 (25), 598 (62), 408 (100). Anal. Calcd for $C_{69}H_{72}Cu_2I_2N_3P_3$ (1415.1): C, 58.48; H, 5.04; N, 2.93. Found: C, 58.05; H, 5.04; N, 2.93.

*[(2-(diphenylphosphino)-4-phenethylpyridine)$_3$Cu$_2$I$_2$] (**17-I**).* Yield: 334 mg, 225 mmol, 62%; yellow powder. IR (ATR): $\tilde{\nu}$ = 3025 (vw), 1587 (w), 1546 (vw), 1495 (vw), 1480 (vw), 1453 (vw), 1434 (w), 1387 (vw), 1094 (vw), 741 (w), 692 (m), 500 (w), 466 (w) cm^{-1}. MS (FAB), *m*/*z* (%): 1270 (2), 1180 (8), 990 (8), 812 (12), 798 (24), 620 (45), 430 (100), 339 (41). Anal. Calcd for $C_{75}H_{66}Cu_2I_2N_3P_3 \cdot 1/2CH_2Cl_2$ (1481.1): C, 59.44; H, 4.43; N, 2.75. Found: C, 59.29; H, 4.48; N, 2.38.

X-ray Crystallography. Crystal structure determinations of **1-I**, **2-I**, **3-I**, **5-I**, **8-I**, **9-I**, **10-I**, **11-I**, **11-I-MTBE**, **14-I**, and **15-I** were performed on a Bruker-Nonius Kappa-CCD diffractometer at 123(2) K and for **1-Cl** on a SMART X2S diffractometer at 200(2) K using Mo

Kα radiation (λ = 0.71073 Å). Crystal data, data collection parameters, and results of the analyses are listed in Table S1, Supporting Information. Direct methods (for **15-I** Patterson methods) were used for structure solution (SHELXS-97),[67] and refinement was carried out using SHELXL-97 (full-matrix least-squares on F^2).[67] Hydrogen atoms were refined using a riding model. A semiempirical absorption correction using equivalent reflections was applied. Single crystals suitable for X-ray diffraction analysis were obtained by slow diffusion of diethyl ether into a solution of the complexes in dichloromethane. In the cases of sparingly soluble complexes crystals were grown by diffusion of diethyl ether into the filtered reaction mixture.

Photophysical Measurements. Steady-state emission spectra were recorded on a FluoroMax-4 spectrofluorometer by Horiba Scientific equipped with a 150 W xenon-arc lamp, excitation and emission monochromators (1200 grooves/nm blazed at 330 (excitation) and 500 nm (emission)), and a Hamamatsu R928 photomultiplier tube. Emission and excitation spectra were corrected for source intensity (lamp and grating) by standard correction curves. Luminescence quantum yields were measured with a Hamamatsu Photonics absolute PL quantum yield measurement system (C9920-02G) equipped with a L9799-01 CW Xenon light source (150 W), monochromator, C7473 photonic multichannel analyzer, integrating sphere, and employing U6039-05 PLQY measurement software (Hamamatsu Photonics, Ltd., Shizuoka, Japan). All solvents used were of spectrometric grade. Degassed samples were prepared by purging with argon for 30 min. UV−vis absorption spectra were measured on a Thermo Scientific Evolution 201 UV−vis spectrophotometer.

Computational Methods. Density functional theory (DFT) using the BP86[68,69] and B3LYP[70,71] functionals was applied to complexes **2-I**, **5-I**, **6-I**, and **10-I**. The def2-SV(P) basis set[72,73] was used. The resolution-of-identity approximation[74−76] was employed in the BP86 calculations. The m4 grid was used for numerical integration. Analytical harmonic vibrational frequency calculations were conducted to verify that the optimized ground-state structures are minima on the potential energy surface. For the excited states, time-dependent density functional theory (TD-DFT) and the spin-flip Tamm-Dancoff approximation (SF-TDA)[77] approach were applied. All calculations were performed with the Turbomole program package version 6.3.[78]

3. RESULTS AND DISCUSSION

3.1. Synthesis. Copper(I) halide complexes exhibit many coordination motifs depending on the coordinating ligand as well as the molar ratios between ligand and metal salt.[42,79] With pyridine-type ligands L and an equimolar stoichiometry the complexes frequently form $[CuXL]_4$ cubane-like structures or one-dimensional ladder chains $[CuXL]_\infty$ consisting of fused Cu_2X_2 subunits.[42,52,80] Changing the stoichiometry to a ratio of 1:1:2 or even 1:1:3 results in either a $[(CuX)_2L_4]$ form of complex with an isolated rhombohedron Cu_2X_2 core or a mononuclear complex $[CuIL_3]$.[42,81,82] Another dimeric structure with a rhombic Cu_2X_2 core featuring the composition $[Cu_2X_2L_2(R_3P)_2]$ can be obtained using a mixed ligand system with bulky ligands like triphenylphosphane blocking further aggregation.[83−86] Nevertheless, due to their di-, oligo-, or polymeric structure, once precipitated from solution, these complexes are usually only sparingly soluble in organic solvents.

Our approach involves phosphane-substituted pyridine heterocycles, combining phosphine and imine functionalities in a single ligand to achieve a straightforward synthetic pathway for preparation of copper(I) halide cluster complexes. For that, N-heterocycles with a diphenylphosphino group in the ortho position to the coordinating imine nitrogen atom were used. The ligands synthesized and examined on their complexation behavior in this work can be divided into two groups (shown in Charts 1 and 2). The first group (type I) includes an unsubstituted 2-diphenylphosphinopyridine ligand **1** as reference ligand which is then modified at the heterocycle moiety with electron donor or acceptor groups, such as dimethylamino or fluorine, in order to study the electronic effects. Furthermore, by synthesizing several quinoline-, isoquinoline-, or quinoxaline-diphenylphosphanes, the conjugated pyridine system has been extended at different positions. Additionally, the pyridine moiety was also replaced with a benzothiazole unit

Chart 1. Type I P^N Ligands Featuring Different Electronic Characteristics

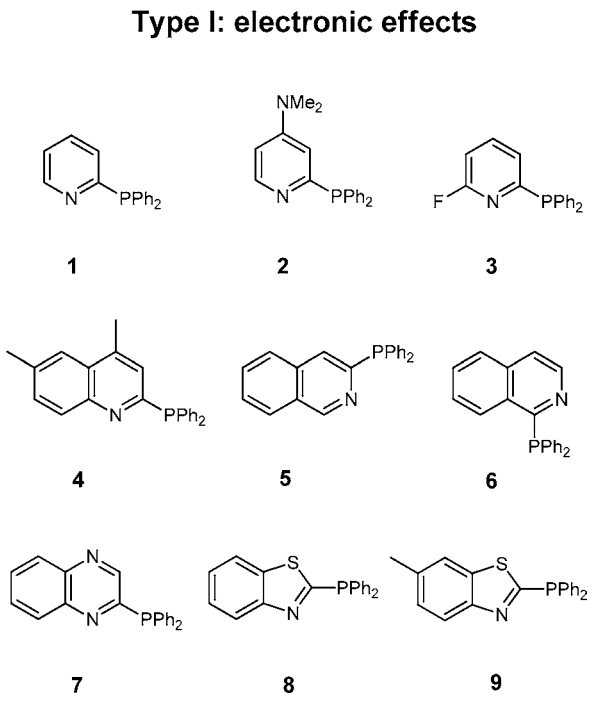

Chart 2. Type II P^N Ligands Featuring Different Alkyl Substituents for Better Solubility and Processability

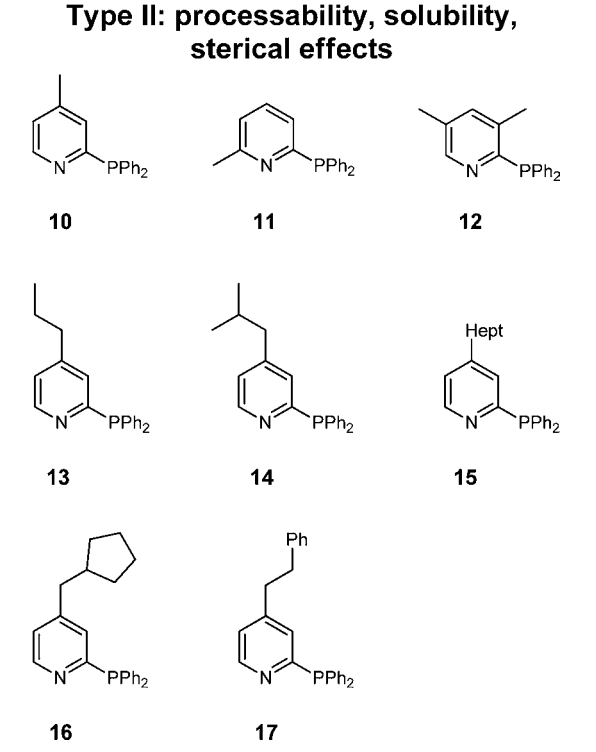

dx.doi.org/10.1021/ic300979c | Inorg. Chem. 2013, 52, 2292−2305

Scheme 1. Synthesis of P^N-Type Ligands 1−17

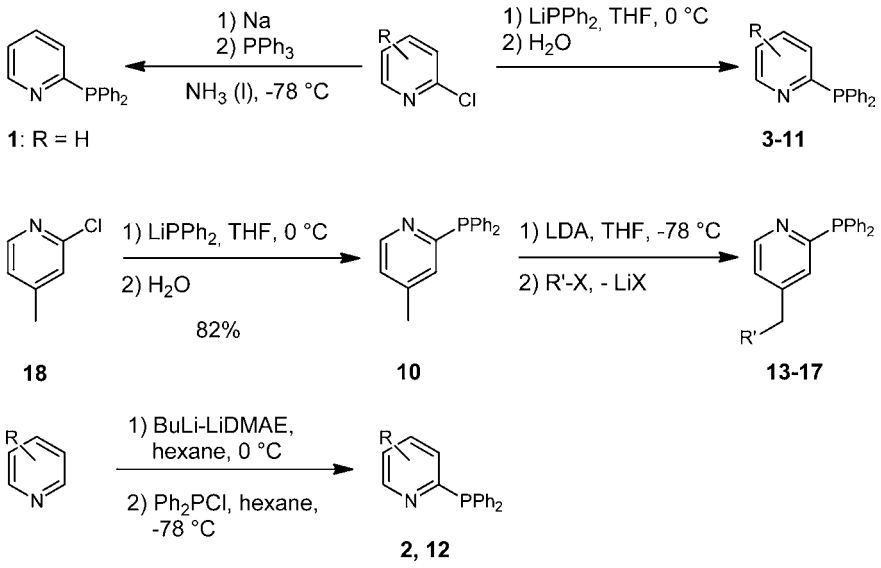

in order to compare it with the pyridine derivatives, and its processability was modified as in the examples below.

The second group (type II) only involves alkyl substituents on the pyridine ring mostly in the 4 position (Chart 2). These are used to adjust the solubility and therefore the processability of these new materials as well as to investigate steric influences. Various alkyl substituents with different chain lengths or branching were introduced to fine tune the solubility of the copper complexes in nonpolar solvents like toluene, xylene, or chlorobenzene which are expected to be the solvents of choice used to process these new materials.

Unsubstituted 2-diphenylphosphinopyridine (**1**) has been prepared via a substitution reaction from 2-chloropyridine and a diphenylphosphino-nucleophile (Scheme 1). During this reaction, the nucleophile $NaPPh_2$ is generated in situ from triphenylphosphane and sodium in liquid ammonia.[64,87,88] A similar procedure is applied for ligands **3**−**11** starting from the appropriate precursor halides using $LiPPh_2$ as nucleophile in tetrahydrofuran at 0 °C. Alkyl-substituted ligands **13**−**17** are accessible in a further reaction sequence, in which the methyl group of 2-(diphenylphosphino)-4-methylpyridine (**10**) can be deprotonated by lithium diisopropylamide and subsequently reacted with different alkyl halides. In a third reaction pathway, substituted 2-diphenylphosphinopyridine ligands can be synthesized via direct C2 lithiation of the corresponding substituted pyridine precursor, followed by addition of chlorodiphenylphosphane as electrophile, which was used for syntheses of ligands **2** and **12** (Scheme 1).[62] All P^N ligands were obtained in moderate to good yields and fully characterized by standard chemical analysis (NMR, MS, IR). It should be noted that synthesis of the ligands as well as synthesis of the complexes (vide infra) does not show any yield-lowering effects when performed in multigram scale.

For the complexation reactions, mostly copper(I) iodide was used as metal salt due to its better oxidation stability compared to copper(I) bromide and copper(I) chloride. However, in terms of investigating the influence of the ligand field strength of different halide anions, copper(I) iodide, copper(I) bromide, and copper(I) chloride were used to obtain the corresponding complexes of ligand **1**, yielding complexes **1-I**, **1-Br**, and **1-Cl**, respectively. The syntheses of the complexes were carried out by mixing the P^N ligands with the respective copper(I) halide in a 3:2 ratio in dichloromethane at room temperature following a literature procedure (Scheme 2).[89] The initially

Scheme 2. General Procedure for Synthesis of Dinuclear Copper(I) Complexes

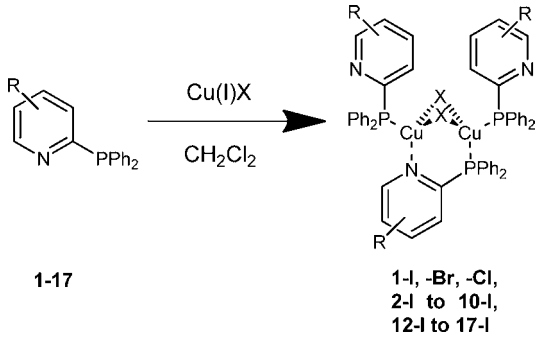

cloudy reaction mixture became clear within hours, indicating the progress of the reaction. Pure materials were obtained upon precipitation with diethyl ether from the filtered reaction mixture and subsequent washing with several organic solvents. The usually high yields dropped with increasing solubility of the complexes. Crystals suitable for X-ray analysis were obtained by slow diffusion of diethyl ether into the reaction mixture as well as into a saturated dichloromethane solution of the appropriate complex. All complexes have been characterized by mass spectroscopy, elemental analysis,[90] and in many cases single-crystal X-ray diffraction, which confirmed a 3:2 ligand to copper stoichiometry for all compounds except for complex **11-I**, which has a 3:1 stoichiometry.

3.2. Structural Studies. The molecular structures of the compounds obtained by X-ray diffraction revealed a butterfly-shaped Cu_2I_2 core surrounded by three ligands. One of the three P^N ligands acts as bridging unit concerning the two copper atoms. The other two ligands coordinate the copper ions only via their phosphorus atom, resulting in a tetrahedral coordination for each metal center. The crystal structure of compound **1-I** is shown in Figure 1. The tetrahedral coordination is typical for mononuclear Cu(I) complexes as

dx.doi.org/10.1021/ic300979c | Inorg. Chem. 2013, 52, 2292−2305

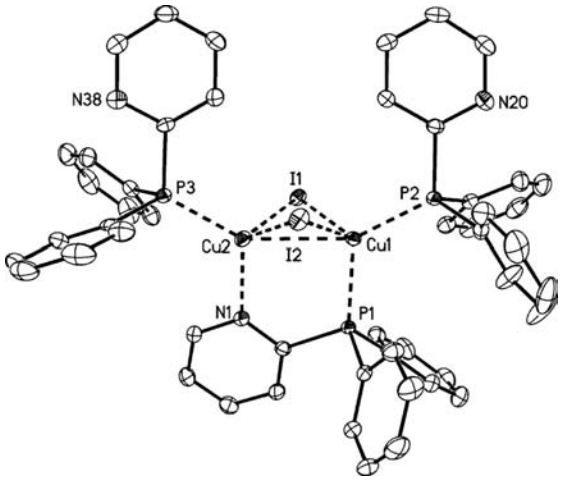

Figure 1. Molecular structure of complex **1-I** (hydrogen atoms are omitted for clarity; displacement parameters are drawn at 50% probability level).

well as for polynuclear Cu(I) clusters, while the butterfly-shaped metal-halide core is in contrast to the typical planar Cu_2X_2 geometry observed for many halogen-bridged Cu_2X_2-type structures.[85,91,92] Interestingly, no intramolecular $\pi\pi$-stacking interactions between any aromatic rings can be observed. The structure of the presented complexes is unprecedented for copper(I), whereas the silver congener $Ag_2Cl_2(pyPPh_2)_2$ was already published in 1982.[93] In general, a coordination geometry with a folded $\{Cu_2(\mu\text{-}X)_2\}$ moiety is rare and could be found for only a few chelating ligands such as naphthyridine,[94] bis(diphenylphosphino)ethane,[95] and (phenylamino)bis(phosphate).[96]

Introduction of various substituents, e.g., methyl (**10-I**), isobutyl (**14-I**), *n*-heptyl (**15-I**), or cyclopentylmethylene (**16-I**), in the 4 position of the pyridine ring does not affect the complexation behavior of these ligands nor does it remarkably change the structural characteristics of the obtained complexes (Figure 2). Also, extension of the aromatic system (e.g., quinoline, quinoxaline, quinaxoline) or alteration of the type of N-heterocycle (e.g., benzothiazole) in the P^N ligands lead to complexes with the prominent butterfly-shaped copper-halide motif with one bridging and two monodentate NP ligands. Notably, substitution only influences the solubility and also the photophysical properties of the synthesized complexes (vide infra).

The copper-copper distance of all measured complexes (2.69−2.83 Å) is in the order of the sum of the van der Waals radii or slightly below (2.80 Å)[97] and therefore too large for significant metallophilic interactions. Furthermore, the distance is basically not affected by changes of the ligands, such as extension of the π systems (**4-I**−**9-I**) or solubility enhancing alkyl groups (**10-I**, **12-I**−**17-I**). The bond distances between the copper and the iodine atoms are nearly identical within one

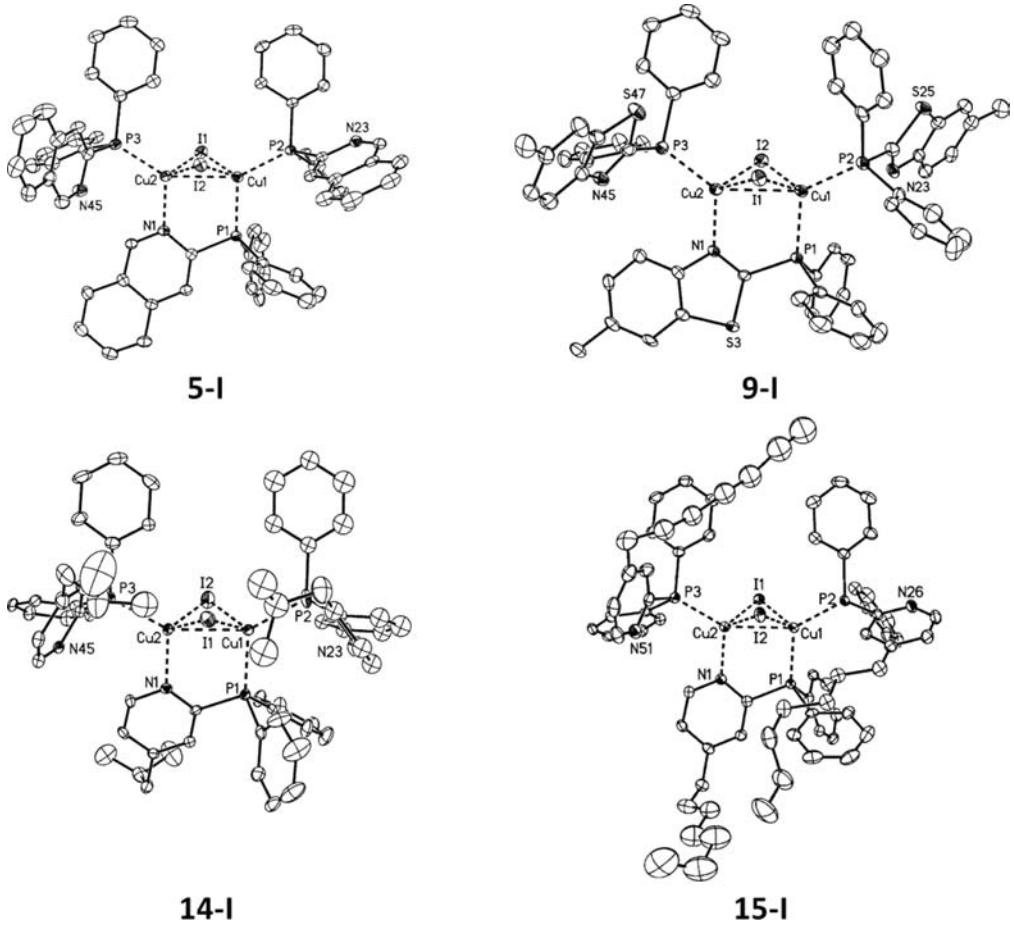

Figure 2. Molecular structures of complexes **5-I**, **9-I**, **14-I**, and **15-I** (hydrogen atoms and minor disordered parts are omitted for clarity; displacement parameters are drawn at 50% probability level).

dx.doi.org/10.1021/ic300979c | *Inorg. Chem.* 2013, 52, 2292−2305

Table 1. Selected Bond Lengths (Angstroms) of Structurally Characterized $(P\hat{}N)_3Cu_2X_2$ Complexes[a]

	1-I	1-Cl	2-I	5-I	9-I
Cu(1)−Cu(2)	2.7694(5)	2.7521(4)	2.7714(8) {2.823}	2.7204(6) {2.751}	2.829(1)
Cu(1)−X(1)	2.6733(7)	2.6383(4)	2.7034(8) {2.746}	2.6930(5) {2.762}	2.658(1)
Cu(1)−X(2)	2.6803(5)	2.6834(4)	2.6717(7) {2.776}	2.6954(5) {2.781}	2.648(1)
Cu(2)−X(1)	2.7280(6)	2.6876(5)	2.6140(7) {2.727}	2.6277(5) {2.727}	2.706(1)
Cu(2)−X(2)	2.6446(5)	2.6818(4)	2.8121(7) {2.854}	2.6802(5) {2.786}	2.698(1)
P(2)−Cu(1)	2.2514(6)	2.242(1)[b]	2.2524(12) {2.3578}	2.2404(9) {2.356}	2.2486(1)
P(1)−Cu(1)	2.2522(7)	2.248(1)[c]	2.2645(13) {2.3573}	2.2555(8) {2.356}	2.2424(16)
P(3)−Cu(2)	2.2507(7)	2.224(1)[d]	2.2443(13) {2.3416}	2.2468(9) {2.348}	2.2429(16)
N(1)−Cu(2)	2.1035(17)	2.106(3)[e]	2.069 (4) {2.1737}	2.076(2) {2.172}	2.069(5)

[a]Calculated bond lengths at the B3LYP/def2-SV(P) level are shown in curly brackets. [b]Cu(2)−P(1). [c]Cu(2)−P(2). [d]Cu(1)−P(3). [e]Cu(1)−N(1).

Table 2. Selected Bond Angles (degrees) of Structurally Characterized $(P\hat{}N)_3Cu_2X_2$ Complexes[a]

	1-I	1-Cl	2-I	5-I	9-I
X(1)−Cu(1)−X(2)	107.63(2)	108.13(1)	110.82(2) {109.42}	108.86(2) {110.2}	108.76(3)
X(1)−Cu(2)−X(2)	107.07(1)	106.74(1)	109.26(2) {107.69}	111.32(2) {111.1}	105.93(3)
Cu(1)−X(1)−Cu(2)	61.68(1)	62.34(1)	62.80(2) {62.12}	61.48(1) {60.2}	63.67(2)
Cu(1)−X(2)−Cu(2)	62.67(1)	61.85(1)	60.65(2) {61.84}	60.80(1) {59.2}	63.90(2)
P(1)−Cu(1)−X(1)	106.31(2)	106.91(4)[b]	107.18(4) {102.2}	106.37(2) {101.7}	102.13(5)
P(1)−Cu(1)−X(2)	104.34(2)	114.12(4)[c]	99.07(4) {104.9}	103.37(2) {104.7}	104.98(5)
P(2)−Cu(1)−P(1)	119.87(2)	119.04(3)	125.39(5) {119.2}	118.16(3) {119.7}	118.55(6)
P(1)−Cu(1)−Cu(2)	87.07(2)	87.55(2)	86.96(4) {84.0}	89.46(2) {84.8}	87.39(5)

[a]Calculated bond angles at the B3LYP/def2-SV(P) level are shown in curly brackets. [b]P(3)−Cu(1)−Cl(1). [c]P(3)−Cu(1)−Cl(1).

particular complex with values ranging from 2.62 to 2.81 Å. Analysis of the relevant bond angles reveals an only slightly distorted tetrahedral geometry around both copper ions, demonstrating the fitting bite angle of this bidentate P^N ligand structure. Bond angles are approaching the tetrahedral standard and reflect the small steric requirements of this ligand system as well as the small constraints that are imposed on the complex structure. Interestingly, the Cu_2X_2 butterfly core almost exhibits a perfectly equilateral Cu_2X triangle with corresponding bond angles very close to 60°. Selected bond lengths and angles are given in Tables 1 and 2.

However, the only modification of the ligands which leads to a completely different coordination behavior is introduction of a methyl group in the 6 position of the pyridine moiety. This can be seen in the case of ligand **11**, which leads to formation of the mononuclear Cu(I) complex **11-I** (Figure 3). Most probably due to the steric demand of this methyl group, a dinuclear structure cannot be formed. In the mononuclear complex, Cu is coordinated by three ligands solely via their phosphorus atom and an iodide ligand yielding a neutral tetrahedral L_3CuI-type complex. Its structural parameters are very similar to the literature-known compound $(Ph_3P)_3CuI$.[98] The corresponding bond angles closely match the tetrahedral angle of 109.5°, and the Cu−P distances are within the range of 2.30−2.31 Å, which is slightly longer than the corresponding distances observed in the dinuclear complexes. For more detailed information about bond lengths or angles of complex **11-I**, see Figure S10 in the Supporting Information.

3.3. Photophysical Characterization at Ambient Temperature. Figure 4 displays the absorption spectra of complexes **6-I** and **10-I** in dichloromethane, along those of the corresponding free ligands **6** and **10**. Complex **6-I** shows

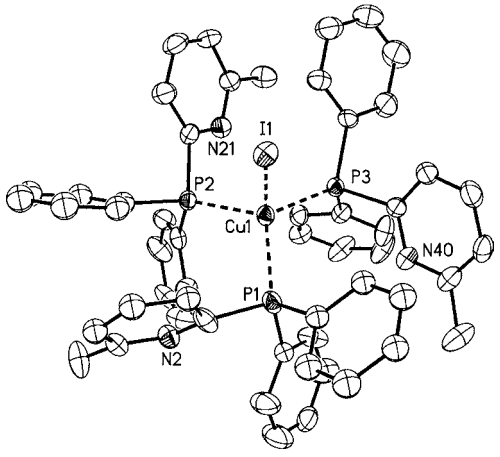

Figure 3. Molecular structure of complex **11-I** (hydrogen atoms, solvent molecule, and minor disordered part are omitted for clarity; displacement parameters are drawn at 50% probability level).

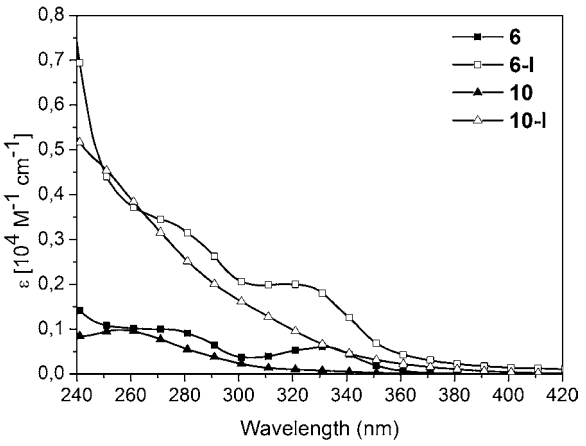

Figure 4. Absorption spectra of complexes **6-I** and **10-I** as well as their corresponding ligands **6** and **10** at ambient temperature in dichloromethane solution.

dx.doi.org/10.1021/ic300979c | Inorg. Chem. 2013, 52, 2292−2305

maxima around 272 (ε = 3400 M^{-1} cm^{-1}) and 319 nm (ε = 2000 M^{-1} cm^{-1}). These are assigned to $\pi-\pi^*$ transitions within the phenyl rings on the phosphane moieties as well as to transitions localized on the isoquinoline moiety, also of $\pi-\pi^*$ character. These assignments are confirmed by comparison with the spectrum of **10-I**. Additionally, a weak shoulder observed for **6-I** at 345 nm, which is not present for the free ligand, indicates an electronic change on one of the isoquinoline moieties. Such a change correlates with the structure of the complex with one of the heterocycles being coordinated. The spectrum of **10-I** is rather unstructured with a broad shoulder around 252 nm, which is assigned to ligand-centered (LC) $\pi-\pi^*$ transitions, being in accordance with the occurrence of a corresponding peak in the free ligand spectrum. The lack of structure is due to a smaller energetic separation between transitions localized on the phenyl rings and the heterocycle, respectively, which is the pyridine versus the energetically lower-lying extended π system of the isoquinoline. In contrast to the structure of the free ligand **10**, the absorption of **10-I** does not show a steep decrease in the absorption coefficient around 300 nm, which is most probably due to the coordinating pyridine moiety of the bridging ligand similar to the discussion of **6-I**. Furthermore, both complexes show tails which are not visible for the free ligands, ranging from approximately 375 to 485 nm and from 371 to 416 nm for complexes **6-I** and **10-I**, respectively (ε = 262−154 M^{-1} cm^{-1}). These low-energy absorptions are assigned to metal-to-ligand charge-transfer (MLCT) transitions mixed with halogen-to-ligand charge-transfer (XLCT) transitions and are therefore assigned to (X+M)LCT states. Electronic absorption maxima and extinction coefficients of compounds **6**, **6-I**, **10**, and **10-I** are summarized in Table 3.

Table 3. Extinction Coefficients of Compounds 6, 6-I, 10, and 10-I[a]

compound	λ_{abs} [nm]	ε [M^{-1} cm^{-1}]	transition
6	274	996	LC, Ph, $\pi-\pi^*$
	289 (sh)	712	LC, isoquinoline, $\pi-\pi^*$
	321 (sh)	526	LC, isoquinoline, $\pi-\pi^*$
6-I	272	3400	LC, Ph, $\pi-\pi^*$
	319	2000	LC, isoquinoline, $\pi-\pi^*$
	345 (sh)	1078	LC, bridging isoquinoline, $\pi-\pi^*$
	375 (sh)	262	(X+M)LCT
10	256	984	Ph, $\pi-\pi^*$
10-I	252 (sh)	4470	LC, Ph, $\pi-\pi^*$
	371 (sh)	154	(X+M)LCT

[a]In dichloromethane solution. sh = shoulder.

These assignments are further supported by theoretical calculations of complexes **2-I**, **5-I**, **6-I**, and **10-I** using density functional theory (DFT) with functionals BP86[68,69] and B3LYP.[70,71] The frontier orbitals for the investigated compounds are shown in Figure 5.

All complexes show a similar trend, with the HOMO being largely localized on the Cu_2X_2 core with some participation of the phosphorus atoms of the monocoordinated ligands. On the other hand, the LUMO is mainly located on the bridging P^N ligand. Therefore, as shown in Table 4, the modifications on the N-heterocycle mainly affect the LUMO energy, while the HOMO energy remains basically unchanged, lying roughly around −4.50 eV. On the basis of these results, the type of electronic transition that leads to the lowest excited states may

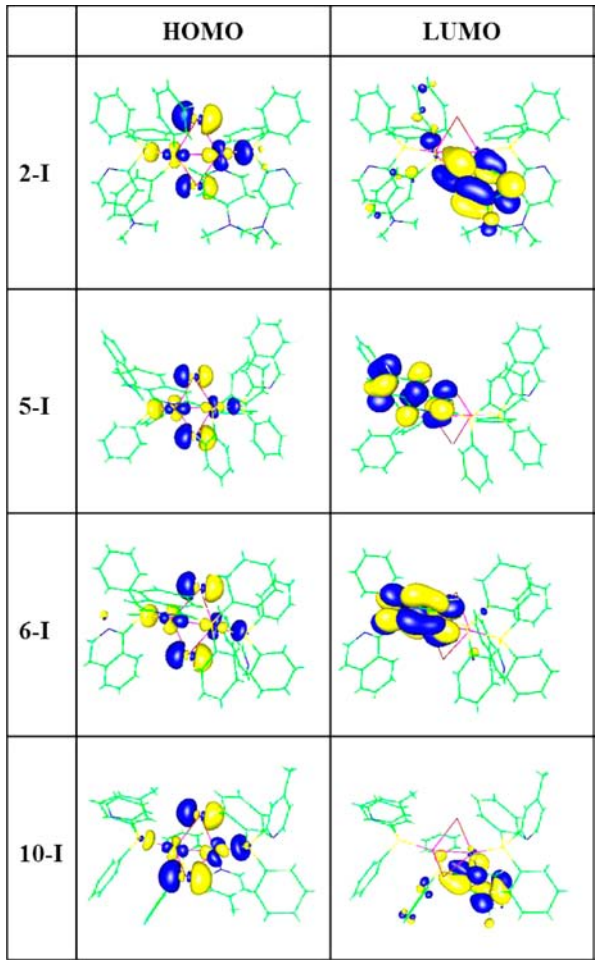

Figure 5. HOMO and LUMO frontier orbital plots of complexes **2-I**, **5-I**, **6-I**, and **10-I** based on DFT calculations.

Table 4. Calculated Orbital Energies[a]

	2-I	5-I	6-I	10-I
HOMO	−4.40	−4.46	−4.55	−4.46
LUMO	−1.01	−1.83	−2.04	−1.83

[a]B3LYP/def2-SV(P) HOMO and LUMO orbital energies (in eV, 1 eV ≙ 8067 cm^{-1}) at the ground-state geometry.

be classified as being largely of (X+M)LCT character. Moreover, it appears that the differences in the observed emission maxima may be explained by the variations in the ligand LUMOs. Hence, a fine tuning of the luminescence properties seems possible by making small chemical modifications on the ligands.

Room-temperature powder emission spectra of compounds **1-I**, **2-I**, **4-I**−**8-I**, and **10-I** are shown in Figure 6. Emission spectra of complexes **3-I**, **9-I**, and **12-I**−**17-I** are omitted for clarity, since they are similar to the profiles of complexes **1-I**, **2-I**, **4-I**−**8-I**, and **10-I** and can be found in Figure S13 in the Supporting Information. For a collection of the photophysical properties see Table 5.

In accordance with the assumption of a charge-transfer nature of the emitting state, emission spectra of all investigated complexes are relatively broad and unstructured. This correlates well with our calculations, i.e., with the HOMO being on the Cu_2X_2 cluster and the LUMO on the bridging ligand.[32] Furthermore, the energetic variation of the LUMO, as seen in

dx.doi.org/10.1021/ic300979c | Inorg. Chem. 2013, 52, 2292−2305

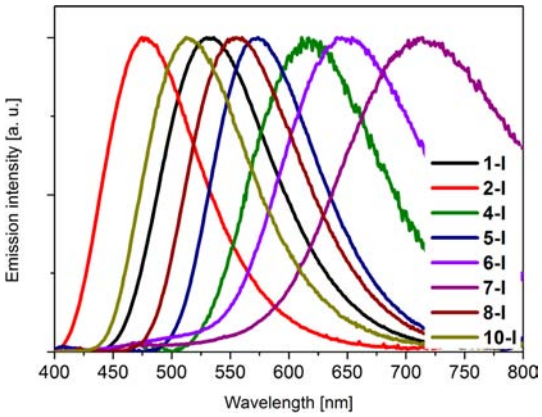

Figure 6. Powder emission spectra of **1-I**, **2-I**, **4-I**–**8-I**, and **10-I** (λ_{exc} = 375 nm, rt). For clarity, emission spectra of complexes **3-I**, **9-I**, and **12-I**–**17-I** can be found separately in Figure S13 in the Supporting Information.

Table 5. Photoluminescence Characteristics[a]

compound	λ_{em} [nm]	Φ_{PL}
1-I	537[b]	0.81
1-Br	550[b]	0.36
1-Cl	569[b]	0.24
2-I	481	0.48
3-I	553	0.59
4-I	605	0.06
5-I	572	0.33
6-I	657	0.16
7-I	713	0.03
8-I	558	0.70
9-I	546	0.94
10-I	523	0.70
12-I	546	0.51
13-I	509	0.74
14-I	497	0.96
15-I	522	0.96
16-I	507	0.96
17-I	545	0.60

[a]Neat powders at rt, λ_{exc} = 375 nm; [b]λ_{exc} = 366 nm

the calculated values (Table 4), is reflected in the emission wavelengths. As discussed on the basis of DFT calculations, modifications of the ligands result mainly in energy alterations of the ligand LUMOs and also of the LUMOs of the corresponding complexes. This characteristic is clearly displayed in the emission spectra of compounds **2-I**, **10-I**, **14-I**, **15-I**, and **16-I**. The corresponding ligands carry electron-donating groups in the 4 position of the pyridine moiety, ranging from weak donors, such as alkyl groups of different length (**10-I**, **14-I**, **15-I**, **16-I**), to a dimethylamino group as strong donor for compound **2-I**. This results in a moderate blue shift for **10-I** and **15-I** of about 15 nm compared to **1-I** and to a sky-blue emission with a band maximum at 481 nm for **2-I**. Consequently, introduction of electron-withdrawing groups such as fluorine or extension of the conjugation on the bridging ligand leads to stabilization of the LUMO and hence a red shift of the emission relative to **1-I** which is visible for complexes **3-I**–**6-I** and **8-I**.

Depending on the position of the extension of the π system on the pyridine ring, the red shift can be rather moderate as for **8-I** (λ_{em} = 558 nm) or large as in the case of **6-I** (λ_{em} = 657 nm). This becomes also apparent for complex **5-I**, which has also an isoquinoline moiety instead of a pyridine moiety but has the phosphino substituent in the 3 instead of the 1 position, resulting in exhibition of a smaller red shift (λ_{em} = 572 nm) as compared to **6-I**. Therefore, it can be assumed that a phosphino substituent in the 1 position of an isoquinoline moiety stabilizes the LUMO more than a substituent in the 3 position. Using quinoline instead of pyridine also results in a red shift of the emission as can be seen for compound **4-I** (λ_{em} = 605 nm). Use of benzothiazoles as coordinating moieties leads to emission maxima at 558 and 546 nm for complexes **8-I** and **9-I**, respectively.

These findings gained from powder measurements together with the results of DFT and TD-DFT calculations show that electron-donating substituents on the pyridine ring, e.g., a dimethylamino group, destabilize the LUMO, consequently leading to a hypsochromic shift of the emission. Conversely, an electron-withdrawing substituent, e.g., a fluorine atom, lowers the LUMO energy, thus shifting the emission to longer wavelengths. Consequently, lowering the energy level of the LUMO by extending the aromatic system also results in a red-shifted emission.

The emission quantum yields in powder are higher than the values reported for similar dinuclear complexes, reaching up to 96% for the alkylated compounds.[32,61,85] These larger quantum yields of **14-I** to **16-I** compared to compound **1-I** with 81% can tentatively be related to a more distinct hindrance due to the alkyl substituents with respect to geometry changes upon excitation. Furthermore, the low emission quantum yield of complex **6-I** (16%) or **7-I** (3%) is probably related to the energy gap law, i.e., a decrease in emission quantum efficiency with decreasing emission energy, since competing nonradiative processes become more relevant.[99]

In Figure 7, the calculated LUMO energies of the ligands are shown as a function of the emission wavelengths of the complexes. The LUMO energies were obtained at the B3LYP/def2-SV(P) level for the optimized free ligand. As visible from the data, there is a linear correlation between those two: a lower, i.e., a more negative, LUMO energy of the ligand is related to a longer emission wavelength. Consequently, for the presented Cu_2X_2 family, the emission color can be roughly estimated based on the calculated LUMO energy of the

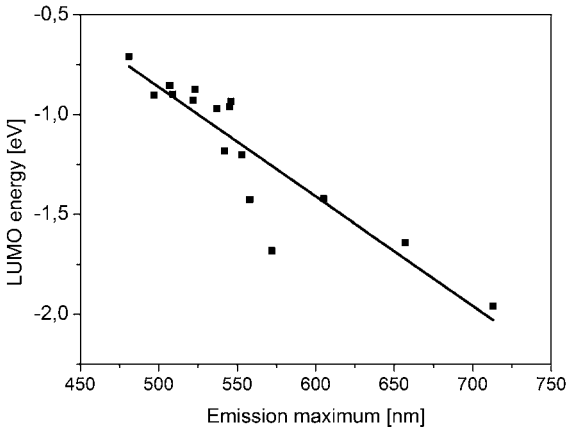

Figure 7. Correlation between ligand LUMO energies and emission maxima of the corresponding complexes (for exact values of the LUMO energy see Table S2 in the Supporting Information).

dx.doi.org/10.1021/ic300979c | Inorg. Chem. 2013, 52, 2292–2305

bridging ligand, enabling a simple design of differently colored emitters.

In order to get further insight into the electronic transitions of this kind of dinuclear complexes, TD-DFT calculations were performed on complexes **2-I**, **5-I**, **6-I**, and **10-I**. A comparison between theoretical and experimental structures for complexes **2-I** and **5-I** is provided in Tables 1 and 2. As is seen, selected calculated bond lengths and angles are in reasonable agreement with X-ray data (vide supra). In Table 6, the HOMO−LUMO gaps are summarized, computed for the geometries optimized for the ground state (S_0) as well as for the first excited singlet (S_1) and triplet states (T_1). Concerning the ground state, the largest gap is found for complex **2-I**, followed by **10-I**, **5-I**, and **6-I** with smaller gaps. According to Table 7, this trend is also observed for the TD-DFT vertical singlet excitation energies (which were only computed with the B3LYP functional), with absorption maxima at 452, 496, 598, and 660 nm for **2-I**, **10-I**, **5-I**, and **6-I**, respectively. The triplet excitation energies differ from the singlet excitation energies only by a few 10^{-2} eV (Table 6).

Table 6. HOMO−LUMO Gaps (in eV) Computed at the BP86/def2-SV(P) and B3LYP/def2-SV(P) Levels for Complexes 2-I, 5-I, 6-I, and 10-I at Their Ground- and Excited-State Equilibrium Geometries

compound	functional	S_0 [eV]	S_1 [eV]	T_1 [eV]
2-I	BP86	1.72	0.80	0.80
	B3LYP	3.39	2.26	2.21
5-I	BP86	1.06	0.59	0.59
	B3LYP	2.63	1.90	*a*
6-I	BP86	0.99	0.51	0.51
	B3LYP	2.50	1.81	1.80
10-I	BP86	1.52	0.73	0.73
	B3LYP	3.15	2.16	2.11

[a]value omitted because of inconsistent data.

Table 7. Vertical Absorptions and Emissions Computed at the TD-B3LYP/def2-SV(P) and SF-TDA/def2-SV(P) Levels for Complexes 2-I, 5-I, 6-I, and 10-I[a]

compound	state	λ_{abs} [nm]	HOMO → LUMO	λ_{em} [nm]	character
2-I	S_1	452	98%	783	99% HOMO → LUMO
	T_1	455	97%	807	98% HOMO → LUMO
				495[b] (*481*)	100% LUMO → HOMO
5-I	S_1	598	99%	873	99% HOMO → LUMO
	T_1	600	98%	891	99% HOMO → LUMO
				547[b] (*572*)	100% LUMO → HOMO
6-I	S_1	660	99%	1028	99% HOMO → LUMO
	T_1	665	98%	1064	98% HOMO → LUMO
				599[b] (*657*)	100% LUMO → HOMO
10-I	S_1	496	98%	834	99% HOMO → LUMO
	T_1	500	97%	875	98% HOMO → LUMO
				512[b] (*523*)	100% LUMO → HOMO

[a]Experimentally observed emission maxima are given in parentheses. [b]Spin-flip Tamm-Dancoff approximation (SF-TDA/def2-SV(P)) single-point calculation at the TD-DFT-optimized triplet geometry.

All calculated excitations show a very distinct charge-transfer (CT) character, and thus, the TD-B3LYP approach is unable to yield quantitatively correct results. CT excited states cannot be described by naïve application of TD-DFT. Nevertheless, the computed absorption wavelengths follow the experimental trend, as indicated by the HOMO−LUMO gaps.

In the case of CT states, it is reported that the spin-flip Tamm-Dancoff approximation (SF-TDA) provides much more accurate phosphorescence energies than TD-DFT.[77] Indeed, the SF-TDA values in Table 7 (given in bold) agree very well with the experimentally observed emission maxima. The computed energies differ only by 5−10% from the experimentally derived values and follow the observed trend. The lowest singlet excited state cannot be described by the SF-TDA approach, but because of the large spatial separation of the two unpaired electrons, we expect this state to be very close to the corresponding triplet state (i.e., within 0.01−0.07 eV as found at the TD-DFT level). Indeed, as can be seen below for compound **1-I**, the singlet-triplet energy separation $\Delta E(S_1-T_1)$ amounts to 400 cm^{-1} (0.05 eV).

In order to examine the influence of halogens on the photoluminescence, the series using 2-(diphenylphosphino)-pyridine as ligand (**1-I**, **1-Br**, **1-Cl**) was examined. As shown in Figure 8, the sequence of the emission maxima (**1-I** 537 nm, **1-Br** 550 nm, **1-Cl** 569 nm) corresponds to the order of ligand field strengths of the halides (I^- < Br^- < Cl^-) leading to a greater splitting of the d orbitals, destabilization of the HOMO, and thus to a reduction of the energy gap.[32] This trend is contrary to the electronegativity of the halides, which should result in a stabilization of the d orbitals due to an increased electron-withdrawing effect. Obviously, the effect of the ligand strength overcompensates the electronegativity. A similar behavior was also found for tetranuclear copper clusters $Cu_4X_4L_4$ (L = substituted pyridine).[100]

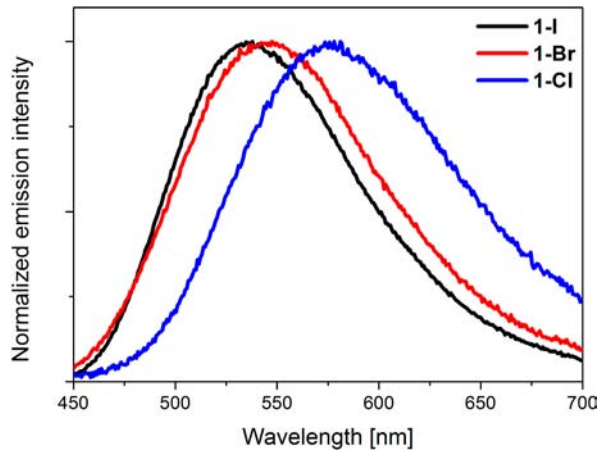

Figure 8. Emission spectra of neat powder of complexes **1-I**, **1-Br**, and **1-Cl**, λ_{exc} = 366 nm, rt.

Influences of different environments on the emission properties have been investigated with the alkylated complexes **10-I**, **14-I**, **15-I**, and **16-I**. Ambient-temperature emission spectra of powders, compounds doped in PMMA, neat thin

dx.doi.org/10.1021/ic300979c | Inorg. Chem. 2013, 52, 2292−2305

films, and dichloromethane solutions, respectively, are shown in Figures 9 and 10 for complexes **10-I** and **16-I** (for complexes

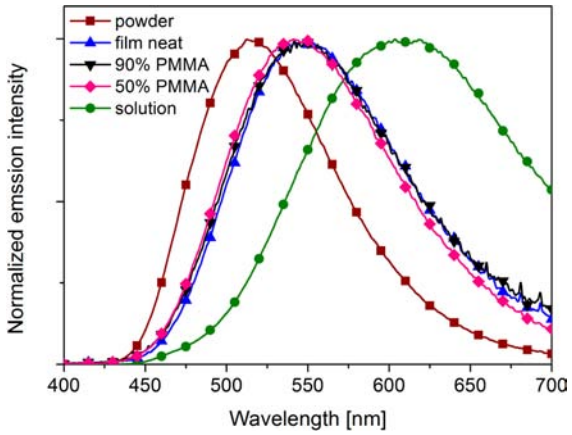

Figure 9. Photoluminescence spectra of complexes **10-I** in different environments: powder, solution, neat film, PMMA doped with 10% emitting compound, PMMA doped with 50% emitting compound: λ_{exc} = 375 nm (powder, solution); 330 nm (films), rt.[101]

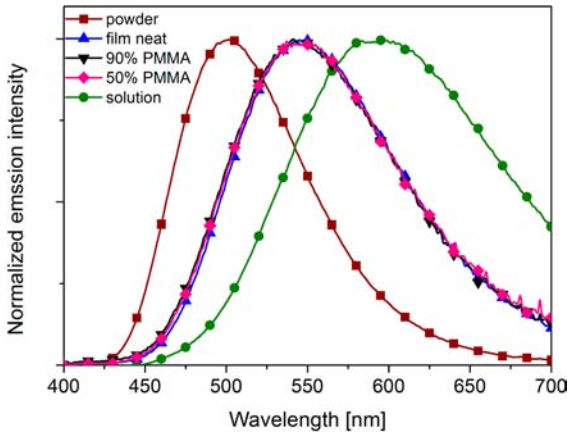

Figure 10. Photoluminescence spectra of complexes **16-I** in different environments: powder, solution, neat film, PMMA doped with 10% emitting compound, PMMA doped with 50% emitting compound: λ_{exc} = 375 nm (powder, solution); 330 nm (films), rt.[101]

14-I and **15-I** see Figures S14 and S15 in the Supporting Information). In Table 8 the corresponding emission maxima as well as the corresponding quantum yields are summarized for compounds **10-I**, **14-I**, **15-I**, and **16-I**. The emission maxima for these complexes investigated as neat powders range from 501 to 522 nm, while the maxima are shifted to longer wavelengths when measured in neat films or doped into PMMA matrices. For the latter case, also a dependence of the doping concentration is found (10%, 50% weight percent of the emitting material: 540−550 nm). The observed red shift is largest when measured in solution exhibiting maxima in the range of 590−610 nm (Table 8).

For neat films as well as for different dopant concentrations in PMMA matrices, the emission maxima almost overlap and exhibit only slight variations in the emission maxima. The emission quantum yields drop considerably when going from neat powders, with ϕ_{PL} values above 80%, to degassed dichloromethane solutions, featuring only about 2% quantum yields (Table 8). The values of the neat films of the complexes **10-I**, **14-I**, **15-I**, and **16-I** lie between 30% and 50% and, thus, are also significantly lower than those measured for the corresponding powders.

Obviously, both the emission wavelengths as well as the photoluminescence quantum yields strongly depend on the environment of the complexes. By influencing the possible extent of structural changes upon excitation, i.e., comparing rigid media like crystals, neat films, and polymer matrices, drastic effects can be observed. In particular, the probabilities of radiationless deactivation are reduced, resulting in significantly higher emission quantum yields for more rigid environments.[44] Solutions, in which those rearrangements upon excitation can occur easily, enhance radiationless deactivation processes leading to a considerable decrease in emission quantum yields. A corresponding behavior being also connected with a drastic decrease of the emission decay time has been described in ref 44. Moreover, the very high emission quantum yields up to 96% in powders may indicate that also quenching processes such as triplet-triplet annihilations (TTA)[102] between adjacent emitter molecules are negligible.[102] This may be explained by relatively small geometry changes in the lowest excited states with subsequent energy reductions even in such rigid systems. For more detailed discussions of these effects see refs 44 and 47.

3.4. Thermally Activated Delayed Fluorescence and Singlet Harvesting with Dinuclear Cu(I) Complexes.

Frequently, Cu(I) complexes represent singlet emitters at ambient temperature, since in these cases a thermally activated delayed fluorescence (TADF) dominates.[44,46,47] In such a situation, the emitter material is potentially highly attractive for application in OLEDs by taking advantage of the singlet-harvesting effect, which is shortly explained: Light generation in an OLED occurs usually in the emission layer after formation of one singlet and three triplet excitons, referring to the ensemble of processes. From these exciton states, fast relaxations lead to populations of the lower excited singlet S_1 and triplet T_1 states of the emitter molecules. In organotransition metal emitters, spin-orbit coupling is usually large enough to induce fast intersystem crossing (ISC) from the S_1 state to the T_1 state. Thus, for large energy separations between the singlet and the

Table 8. Luminescence Properties of Complexes 10-I, 14-I, 15-I, and 16-I in Different Environments

	10-I		14-I		15-I		16-I	
complex	λ_{max}[a] [nm]	Φ_{PL}	λ_{max}[a] [nm]	Φ_{PL}	λ_{max}[a] [nm]	Φ_{PL}	λ_{max}[a] [nm]	Φ_{PL}
powder	515	0.83	514	0.96	522	0.96	501	0.96
neat film	548	0.35	550	0.28	548	0.31	546	0.50
90% PMMA[b]	547	0.34	540	0.47	549	0.31	545	0.31
50% PMMA[b]	543	0.28	542	0.40	550	0.37	546	0.34
CH_2Cl_2 solution	608	0.02	590	0.02	595	0.02	594	0.02

[a] λ_{exc} = 375 nm (powder, solution); 330 nm (films), rt. [b] Weight percent.

dx.doi.org/10.1021/ic300979c | Inorg. Chem. 2013, 52, 2292−2305

triplet states, $\Delta E(S_1-T_1)$, for example amounting to several 10^3 cm^{-1}, only a triplet emission is observed at ambient temperature. Applied in OLEDs, this leads to the well-known *triplet-harvesting effect*.[23] On the other hand, for small energy separations, for example, of $\Delta E(S_1-T_1)$ being only several 10^2 cm^{-1}, thermal activation or up-ISC processes will occur at ambient temperature from the T_1 state to the S_1 state. Subsequently and under suitable conditions, almost all light emission will stem from the singlet S_1 state, representing the *singlet-harvesting effect*.[44,46,47] The corresponding emission is not a spontaneous fluorescence, since the S_1 state population is fed by the T_1 reservoir. Therefore, the resulting emission exhibits a longer decay time than that of the prompt fluorescence, representing the thermally activated delayed fluorescence.

The Cu(I) complex **1-I**, as displayed in Figure 1, has been investigated as a representative example.[103] Figure 11

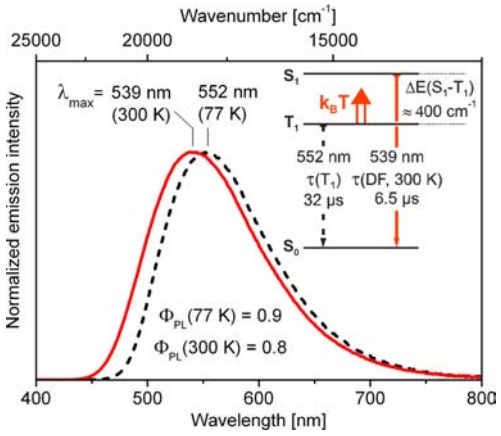

Figure 11. Emission spectra, quantum yields, and decay times of the dinuclear Cu(I) complex **1-I** (powder) as displayed in Figure 1. Inset symbolizes that the emission at ambient temperature represents a thermally activated delayed fluorescence (TADF), exhibiting a decay time of $\tau(DF) = 6.5$ μs. k_BT stands for the thermal energy, being available at a given temperature T.

summarizes a series of emission data of the powder material. At $T = 77$ K, a broad emission band, peaking at λ_{max} (77 K) = 552 nm, is observed. The emission decay, exhibiting a time constant of $\tau(77\ K) = 32$ μs, is monoexponential and ascribed to a phosphorescence stemming from the T_1 state. With this decay time and the measured emission quantum yield of $\phi_{PL}(77\ K) = 0.9$, a radiative decay of $k^r(T_1) = \phi_{PL}/\tau(T_1) = 2.8 \times 10^4$ s^{-1} is calculated.

With temperature increase to $T = 300$ K, a blue shift of the emission maximum of ~13 nm is observed, which corresponds to about 4×10^2 cm^{-1}. We assign this ambient-temperature emission to result from the thermally activated S_1 state. Almost the same activation energy is determined from the temperature dependence of the emission decay time. It decreases monotonically over the whole temperature range from 77 to 300 K and thus excludes a possible misinterpretation according to an occurrence of a phase transition in that range. The emission quantum yield at $T = 300$ K of $\phi_{PL} = 0.8$ is only slightly lower than that at 77 K. With the measured decay time of $\tau(300\ K) = \tau(DF) = 6.5$ μs, a radiative decay rate of $k^r(DF) = 1.2 \times 10^5$ s^{-1} is obtained. The growing in of the radiative rate by more than a factor of 4 with temperature increase is a consequence of the thermally activated additional decay channel via the $S_1 \rightarrow S_0$ emission.

In conclusion, the thermally activated singlet harvesting renders Cu(I) complexes to be attractive OLED emitters. The very long emission decay time of the triplet state would not allow for an application as triplet emitters, since the roll-off of the OLED efficiency would be too large, for example, due to significant saturation effects. On the other hand, a decay time of the delayed fluorescence of $\tau(DF) = 6.5$ μs for the discussed example is already similarly short as found for Pt(II) complexes which can be applied with good efficiencies in OLEDs[15,18] Moreover, Cu(I) complexes offer the future potential for designing materials with even smaller $\Delta E(S_1-T_1)$ energy separations. Possibly, this might lead to materials that would exhibit even larger radiative decay rates (or shorter emission decay times) than $Ir(ppy)_3$, exhibiting a value of $k^r(T_1) \approx 7 \times 10^5$ s^{-1} ($\tau(T_1) = 1.4$ μs).[11] In summary, the low-cost copper-based complexes seem to develop to interesting OLED emitter materials.

4. CONCLUSION

Highly luminescent dinuclear Cu(I) complexes have been synthesized employing a modular approach, consisting of a butterfly-shaped Cu_2X_2 core and three P^N-type ligands. One of the ligands acts as a bridge between the two Cu(I) centers, whereas the other two only coordinate via the phosphorus atom as revealed by single-crystal X-ray diffraction. The photoluminescence properties depend distinctly on the substitution pattern at the pyridine moiety. Neat complex powders feature photoluminescence maxima from the blue to the red region of the visible spectrum depending on the electronic characteristics of the corresponding ligand. It is shown that an electron-donating substituent on the pyridine ring, e.g., a dimethylamino group, raises the LUMO to a higher energy level, consequently leading to a blue shift of the photoluminescence maximum. Conversely, an electron-withdrawing substituent stabilizes the LUMO, thus shifting the emission to longer wavelengths. Similarly, by enlarging the aromatic system of the ligands an energy reduction of the LUMO is obtained, which also leads to a red shift of the photoluminescence maximum. These changes were further investigated and confirmed by TD-DFT calculations, revealing that the HOMO energy stays roughly at −4.5 eV while changes in the LUMO energies are more pronounced.

Moreover, emission of the copper(I) complexes exhibits a strong dependence on the rigidity of their immediate environment, as shown by investigating the compounds as neat powders, neat films, in solution, and doped in PMMA matrices. This behavior is related to a geometry change that can occur upon excitation and thus depends on the available space in a matrix or on the flexibility of the environment.

Most remarkably are the high emission quantum yields of some of the investigated complexes of up to $\phi_{PL} = 96\%$ and the relatively short emission decay times of the thermally activated delayed fluorescence of only a few microseconds. Together with the calculated and experimentally determined small energy gap between the S_1 and T_1 states of a few 10^2 cm^{-1}, these complexes may qualify as highly attractive candidates for singlet-harvesting emitters in OLEDs.

dx.doi.org/10.1021/ic300979c | Inorg. Chem. 2013, 52, 2292−2305

■ ASSOCIATED CONTENT

Supporting Information

X-ray crystallography data for complexes **1-I**, **2-I**, **3-I**, **5-I**, **8-I**, **9-I**, **10-I**, **11-I**, **14-I**, **15-I**, **11-I-MTBE**, and **1-Cl** in CIF format; spectroscopic data of compounds **3**−**5**, **7**, **9**, **10**, **12**−**17**, additional photophysical spectra of complexes **3-I**, **9-I**, and **12-I**−**17-I**, X-ray crystallographic data for **1-I**, **2-I**, **3-I**, **5-I**, **8-I**, **9-I**, **10-I**, **11-I**, **14-I**, **15-I** (CCDC 838846−838855), **11-I-MTBE** (CCDC 878649), and **1-Cl** (CCDC 876712) together with Cartesian coordinates (in Angstroms) of the optimized BP86/def2-SV(P) and B3LYP/def2-SV(P) ground-state equilibrium geometries of compounds **2-I**, **5-I**, **6-I**, and **10-I**. This material is available free of charge via the Internet at http://pubs.acs.org.

■ AUTHOR INFORMATION

Corresponding Author

*E-mail: baumann@cynora.com; uwe.monkowius@jku.at; hartmut.yersin@chemie.uni-regensburg.de; braese@kit.edu.

Notes

The authors declare no competing financial interest.

■ ACKNOWLEDGMENTS

We acknowledge financial support from KIT. We also thank the Deutsche Forschungsgemeinschaft (DFG) for support, through projects B2 and C1 of SFB/TRR 88 and the Bundesministerium für Bildung und Forschung (BMBF). Furthermore, we also thank Lena-Maria Fleig, Dominik Pfaff (Institute of Organic Chemistry), and Dr. Mathias Mydlak (cynora GmbH) for their support.

■ REFERENCES

(1) So, F.; Kido, J.; Burrows, P. *MRS Bull.* **2008**, *33*, 663−669.
(2) Yersin, H., Ed. *Highly Efficient OLEDs with Phosphorescent Materials*; Wiley-VCH: Weinheim, 2008.
(3) He, L.; Qiao, J.; Duan, L.; Dong, G.; Zhang, D.; Wang, L.; Qiu, Y. *Adv. Funct. Mater.* **2009**, *19*, 2950−2960.
(4) Tsuzuki, T.; Tokito, S. *Adv. Mater.* **2007**, *19*, 276−280.
(5) Yang, C.-H.; Cheng, Y.-M.; Chi, Y.; Hsu, C.-J.; Fang, F.-C.; Wong, K.-T.; Chou, P.-T.; Chang, C.-H.; Tsai, M.-H.; Wu, C.-C. *Angew. Chem., Int. Ed.* **2007**, *46*, 2418−2421.
(6) Lowry, M. S.; Bernhard, S. *Chem.—Eur. J.* **2006**, *12*, 7970−7977.
(7) Ulbricht, C.; Beyer, B.; Friebe, C.; Winter, A.; Schubert, U. S. *Adv. Mater.* **2009**, *21*, 4418−4441.
(8) Lamansky, S.; Djurovich, P. I.; Murphy, D.; Abdel-Razzaq, F.; Kwong, R.; Tsyba, I.; Bortz, M.; Mui, B.; Bau, R.; Thompson, M. E. *Inorg. Chem.* **2001**, *40*, 1704−1077.
(9) Flamigni, L.; Barbieri, A.; Sabatini, C.; Ventura, B.; Barigelletti, F. *Top. Curr. Chem.* **2007**, *281*, 143−203.
(10) Yersin, H.; Rausch, A. F.; Czerwieniec, R. In *Physics of Organic Semiconductors*; Bruetting, W., Adachi, C., Holmes, R. J., Eds.; Wiley-VCH: Weinheim, 2012; p 371.
(11) Hofbeck, T.; Yersin, H. *Inorg. Chem.* **2010**, *49*, 9290−9299.
(12) Zhou, G.-J.; Wang, X.-Z.; Wong, W.-Y.; Yu, X.-M.; Kwok, H.-S.; Lin, Z. *J. Organomet. Chem.* **2007**, *692*, 3461−3473.
(13) Wong, W.-Y.; He, Z.; So, S.-K.; Tong, K.-L.; Lin, Z. *Organometallics* **2005**, *24*, 4079−4082.
(14) Che, C.-M.; Kwok, C.-C.; Lai, S.-W.; Rausch, A., F.; Finkenzeller, W., J.; Zhu, N.; Yersin, H. *Chem.—Eur. J.* **2010**, *16*, 233−247.
(15) Rausch, A., F.; Murphy, L.; Williams, J. A. G.; Yersin, H. *Inorg. Chem.* **2012**, *51*, 312−319.
(16) Williams, J. A. G. *Top. Curr. Chem.* **2007**, *281*, 205−268.
(17) Williams, J. A. G.; Develay, S.; Rochester, D. L.; Murphy, L. *Coord. Chem. Rev.* **2008**, *252*, 2596−2611.
(18) Kalinowski, J.; Fattori, V.; Cocchi, M.; Williams, J. A. G. *Coord. Chem. Rev.* **2011**, *255*, 2401−2425.
(19) Kim, J. H.; Liu, M. S.; Jen, A. K.-Y.; Carlson, B.; Dalton, L. R.; Shu, C.-F.; Dodda, R. *Appl. Phys. Lett.* **2003**, *83*, 776−778.
(20) Lu, J.; Tao, Y.; Chi, Y.; Tung, Y. *Synth. Met.* **2005**, *155*, 56−62.
(21) Chou, P.-T.; Chi, Y. *Eur. J. Inorg. Chem.* **2006**, 3319−3332.
(22) Breu, J.; Kratzer, C.; Yersin, H. *J. Am. Chem. Soc.* **2000**, *122*, 2548−2555.
(23) Yersin, H. *Top. Curr. Chem.* **2004**, *241*, 1−26.
(24) Barbieri, A.; Accorsi, G.; Armaroli, N. *Chem. Commun.* **2008**, *19*, 2185−2193.
(25) Hsu, C.-W.; Lin, C.-C.; Chung, M.-W.; Chi, Y.; Lee, G.-H.; Chou, P.-T.; Chang, C.-H.; Chen, P.-Y. *J. Am. Chem. Soc.* **2011**, *133*, 12085−12099.
(26) Czerwieniec, R.; Hofbeck, T.; Crespo, O.; Laguna, A. M.; Gimeno, M. C.; Yersin, H. *Inorg. Chem.* **2010**, *49*, 3764−3767.
(27) Barakat, K. A.; Cundari, T. R.; A., M. *J. Am. Chem. Soc.* **2003**, *125*, 14228−14229.
(28) Igawa, S.; Hashimoto, M.; Kawata, I.; Hoshino, M.; Osawa, M. *Inorg. Chem.* **2012**, *51*, 5805−5813.
(29) Zink, D. M.; Baumann, T.; Nieger, M.; Barnes, E. C.; Klopper, W.; Bräse, S. *Organometallics* **2011**, *30*, 3275−3283.
(30) Zhang, L.; Li, B.; Su, Z. *J. Phys. Chem. C.* **2009**, *113*, 13968−13973.
(31) Che, G.; Su, Z.; Li, W.; Chu, B.; Li, M.; Hu, Z.; Zhang, Z. *Appl. Phys. Lett.* **2006**, *89*, 103511/1−103511/3.
(32) Tsuboyama, A.; Kuge, K.; Furugori, M.; Okada, S.; Hoshino, M.; Ueno, K. *Inorg. Chem.* **2007**, *46*, 1992−2001.
(33) Manbeck, G. F.; Brennessel, W. W.; Eisenberg, R. *Inorg. Chem.* **2011**, *50*, 3431−3441.
(34) McMillin, D. R.; Buckner, M. T.; Ahn, B. T. *Inorg. Chem.* **1977**, *16*, 943−945.
(35) Buckner, M. T.; McMillin, D. R. *J. Chem. Soc., Chem. Commun.* **1978**, 759−761.
(36) Blaskie, M. W.; McMillin, D. R. *Inorg. Chem.* **1980**, *19*, 3519−3522.
(37) McMillin, D. R.; Kirchhoff, J. R.; Goodwin, K. V. *Coord. Chem. Rev.* **1985**, *64*, 83−92.
(38) McMillin, D. R.; McNett, K. M. *Chem. Rev.* **1998**, *98*, 1201−1219.
(39) Crane, D. R.; DiBenedetto, J.; Palmer, C. E. A.; McMillin, D. R.; Ford, P. C. *Inorg. Chem.* **1988**, *27*, 3698−3700.
(40) Simon, J. A.; Palke, W. E.; Ford, P. C. *Inorg. Chem.* **1996**, *35*, 6413−6421.
(41) Crestani, M. G.; Manbeck, G. F.; Brennessel, W. W.; McCormick, T. M.; Eisenberg, R. *Inorg. Chem.* **2011**, *50*, 7172−7188.
(42) Ford, P. C.; Cariati, E.; Bourassa, J. *Chem. Rev.* **1999**, *99*, 3625−3647 and references therein.
(43) Hashimoto, M.; Igawa, S.; Yashima, M.; Kawata, I.; Hoshino, M.; Osawa, M. *J. Am. Chem. Soc.* **2011**, *133*, 10348−10351.
(44) Czerwieniec, R.; Yu, J.; Yersin, H. *Inorg. Chem.* **2011**, *50*, 8293−8301.
(45) Czerwieniec, R.; Yu, J.; Yersin, H. *Inorg. Chem.* **2012**, *51*, 1975.
(46) Yersin, H.; Czerwieniec, R.; Hupfer, A. Singlet harvesting with brightly emitting Cu(I) and metal-free organic compounds. *Proc. SPIE* **2012**, 843508.
(47) Yersin, H.; Rausch, A. F.; Czerwieniec, R.; Hofbeck, T.; Fischer, T. *Coord. Chem. Rev.* **2011**, *255*, 2622−2652.
(48) Gushurst, A. K. I.; McMillin, D. R.; Dietrich-Buchecker, C. O.; Sauvage, J. P. *Inorg. Chem.* **1989**, *28*, 4070−4072.
(49) Miller, M. T.; Gantzel, P. K.; Karpishin, T. B. *J. Am. Chem. Soc.* **1999**, *121*, 4292−4293.
(50) Cuttel, D. G.; Kuang, S.-M.; Fanwick, P. E.; McMillin, D. R.; Walton, R. A. *J. Am. Chem. Soc.* **2002**, *124*, 6−7.
(51) Zhang, Q.; Ding, J.; Cheng, Y.; Wang, L.; Xie, Z.; Jing, X.; Wang, F. *Adv. Funct. Mater.* **2007**, *17*, 2983−2990.
(52) Kyle, K. R.; Ryu, C. K.; DiBenedetto, J. A.; Ford, P. C. *J. Am. Chem. Soc.* **1991**, *113*, 2954−2965.

(53) Parker, C. A.; Hatchard, C. G. *Trans. Faraday Soc.* **1961**, *57*, 1864−1904.
(54) Parker, C. A.; Hatchard, C. G. *J. Phys. Chem.* **1962**, *66*, 2506−2511.
(55) Saltiel, J.; Curtis, H. C.; Metts, L.; Miley, J. W.; Winterle, J.; Wrighton, M. *J. Am. Chem. Soc.* **1970**, *92*, 410−411.
(56) Endo, A.; Sato, K.; Yoshimura, K.; Kai, T.; Kawada, A.; Miyazaki, H.; Adachi, C. *Appl. Phys. Lett.* **2011**, *98*, 083302/1−083302/3.
(57) Goushi, K.; Yoshida, K.; Adachi, C. *Nat. Photonics* **2012**, *6*, 253−258.
(58) Felder, D.; Nierengarten, J.-F.; Barigelletti, F.; Ventura, B.; Armaroli, N. *J. Am. Chem. Soc.* **2001**, *123*, 6291−6299.
(59) Zhang, Q.; Zhou, Q.; Cheng, Y.; Wang, L.; Ma, D.; Jing, X.; Wang, F. *Adv. Mater.* **2004**, *16*, 432−436.
(60) Deaton, J. C.; Switalski, S. C.; Kondakov, D. Y.; Young, R. H.; Pawlik, T. D.; Giesen, D. J.; Harkins, S. B.; Miller, A. J. M.; Mickenberg, S. F.; Peters, J. C. *J. Am. Chem. Soc.* **2010**, *132*, 9499−9508.
(61) Liu, Z.; Qayyum, M. F.; Wu, C.; Whited, M. T.; Djurovich, P. I.; Hodgson, K. O.; Hedman, B.; Solomon, E. I.; Thompson, M. E. *J. Am. Chem. Soc.* **2011**, *133*, 3700−3703.
(62) Cuperly, D.; Gros, P.; Fort, Y. *J. Org. Chem.* **2002**, *67*, 238−241.
(63) Brück, A.; Ruhland, K. *Organometallics* **2009**, *28*, 6383−6401.
(64) Monkowius, U.; Zabel, M.; Fleck, M.; Yersin, H. *Z. Naturforsch.* **2009**, *64b*, 1513−1524.
(65) Moore, S. S.; Whitesides, G. M. *J. Org. Chem.* **1982**, *47*, 1489−1493.
(66) Grotjahn, D. B.; Lev, D. A. *J. Am. Chem. Soc.* **2004**, *126*, 12232−12233.
(67) Sheldrick, G. M. *Acta Crystallogr.* **2008**, *A64*, 112−122.
(68) Becke, A. D. *Phys. Rev. A* **1988**, *38*, 3098−3100.
(69) Perdew, J. P. *Phys. Rev. B* **1986**, *33*, 8822−8827.
(70) Lee, C.; Yang, W.; Parr, R. G. *Phys. Rev. B* **1988**, *37*, 785−789.
(71) Stephens, P. J.; Devlin, F. J.; Chabalowski, C. F.; Frisch, M. J. *J. Phys. Chem.* **1994**, *98*, 11623−11627.
(72) Weigend, F.; Ahlrichs, R. *Phys. Chem. Chem. Phys.* **2005**, *7*, 3297−3305.
(73) Rappoport, D.; Furche, F. *J. Chem. Phys.* **2010**, *133*, 134105/1−134105/11.
(74) Häser, M.; Ahlrichs, R. *J. Comput. Chem.* **1989**, *10*, 104−111.
(75) Weigend, F.; Häser, M. *Theor. Chem. Acc.* **1997**, *97*, 331−340.
(76) Sierka, M.; Hogekamp, A.; Ahlrichs, R. *J. Chem. Phys.* **2003**, *118*, 9136−9148.
(77) Kühn, M.; Weigend, F. *Chem. Phys. Chem.* **2011**, *12*, 3331−3336.
(78) TURBOMOLE V6.3 2011, a development of University of Karlsruhe and Forschungszentrum Karlsruhe GmbH, 1989−2007, TURBOMOLE GmbH, since 2007; available from http://www.turbomole.com.
(79) Eisler, D. J.; Kirby, C. W.; Puddephatt, R. J. *Inorg. Chem.* **2003**, *42*, 7626−7634 and references therein.
(80) Fitchett, C. M.; Steel, P. J. *Inorg. Chem. Commun.* **2007**, *10*, 1297−1300.
(81) Schramm, V.; Pierre, A.; Hiller, W. *Acta Crystallogr.* **1984**, *C40*, 1840−1841.
(82) Hiller, W. *Acta Crystallogr.* **1986**, *C42*, 149−150.
(83) Engelhardt, L. M.; Healy, P. C.; Kildea, J. D.; White, A. H. *Aust. J. Chem.* **1989**, *42*, 913−922.
(84) Maeyer, J. T.; Johnson, T. J.; Smith, A. K.; Borne, B. D.; Pike, R. D.; Pennington, W. T.; Krawiec, M.; Rheingold, A. L. *Polyhedron* **2003**, *22*, 419−431.
(85) Araki, H.; Tsuge, K.; Sasaki, Y.; Ishizaka, S.; Kitamura, N. *Inorg. Chem.* **2005**, *44*, 9667−9675.
(86) Hirtenlehner, C.; Monkowius, U. *Inorg. Chem. Commun.* **2012**, *15*, 109−112.
(87) Mackewitz, T.; Volland, M.; Paciello, R.; Schäfer, A.; Breit, B.; Seiche, W. DE 10 2004 014 474 A1, 2004.10.21, 2004.
(88) Feltham, R. D.; Gary, H. *J. Organomet. Chem.* **1971**, *33*, 347−355.
(89) Yersin, H.; Fischer, T.; Monkowius, U.; Hofbeck, T. DE 10 2009 030 475 A1.
(90) The complexes tend to include solvent molecules, which cannot be removed completely. In addition, some of the complexes have a low solubility in most common organic solvents which hampers purification by recrystallisation. Therefore, a highly accurate elemental analysis cannot be achieved.
(91) Aslanidis, P.; Cox, P. J.; Divanidis, S.; Tsipis, A. C. *Inorg. Chem.* **2002**, *41*, 6875−6886.
(92) Henary, M.; Wootton, J. L.; Khan, A. I.; Zink, J. I. *Inorg. Chem.* **1997**, *36*, 796−801.
(93) Alcock, N. W.; Moore, P.; Lampe, P. A.; Mok, K. F. *J. Chem. Soc., Dalton Trans.* **1982**, 207−210.
(94) Araki, H.; Tsuge, K.; Sasaki, Y.; Ishizaka, S.; Kitamura, N. *Inorg. Chem.* **2007**, *46*, 10032−10034.
(95) Lobana, T. S.; Sharma, R.; Bermejo, E.; Castineiras, A. *Inorg. Chem.* **2003**, *42*, 7728−7730.
(96) Ganesamoorthy, C.; Balakrishna, M. S.; George, P. P.; Mague, J. T. *Inorg. Chem.* **2007**, *46*, 848−858.
(97) Bondi, A. *J. Phys. Chem.* **1964**, *68*, 441−451.
(98) Barron, P. F.; Dyason, J. C.; Healy, P. C.; Engelhardt, L. M.; Pakawatchai, C.; Patrick, V. A.; White, A. H. *J. Chem. Soc., Dalton Trans.* **1987**, 1099−1106.
(99) Cunningham, C. T.; Cunningham, K. L. H.; Michalec, J. F.; McMillin, D. R. *Inorg. Chem.* **1999**, *38*, 4388−4392.
(100) Ryu, C. K.; Vitale, M.; Ford, P. C. *Inorg. Chem.* **1993**, *32*, 869. Vitale, M.; Ryu, C. K.; Palke, W. E.; Ford, P. C. *Inorg. Chem.* **1994**, *33*, 561.
(101) NMR spectra of only a few complexes with sufficient solubility could be measured and feature very broad signals indicative of a fluxional behavior of the ligand sphere. In addition, in the mass spectra no signals representing the ions of the complete complexes could be detected. Therefore, the identity of the solution species is not without doubt. However, due to the similar emission peaks we assume that the complex molecules are identical both in solution and in the solid state.
(102) Tanaka, Y.; Azumi, T. *Inorg. Chem.* **1986**, *25*, 247−248.
(103) Complexes **1-Cl** and **1-Br** show similar properties as **1-I**. Corresponding data will be presented elsewhere.